ACS APPLIED MATERIALS & INTERFACES

Energy, Environmental, and Catalysis Applications

Zn-Promoted Selective Gas Phase Hydrogenation of Tertiary and Secondary C4 Alkynols over Supported Pd

Alberto González-Fernández, Ángel Berenguer-Murcia, Diego Cazorla-Amoros, and Fernando Cárdenas-Lizana

ACS Appl. Mater. Interfaces, **Just Accepted Manuscript** • DOI: 10.1021/acsami.0c05285 • Publication Date (Web): 01 Jun 2020

Zn-Promoted Selective Gas Phase Hydrogenation of Tertiary and Secondary C4 Alkynols over Supported Pd

Alberto González-Fernández[1],

Ángel Berenguer-Murcia[2], *Diego Cazorla-Amorós*[2]

and Fernando Cárdenas-Lizana[1,*]

[1]Chemical Engineering, School of Engineering and Physical Sciences, Heriot-Watt University, Edinburgh EH14 4AS, Scotland, UK

[2]Instituto Universitario de Materiales de Alicante y Departamento de Química Inorgánica, Universidad de Alicante, Ctra. San Vicente del Raspeig s/n, Ap. 99, 03080 Alicante, Spain

Key words: Selective gas phase hydrogenation; 2-methyl-3-butyn-2-ol; 3-butyn-2-ol; hydrogen partial pressure; support effects; PdZn alloy.

ABSTRACT

We have investigated the gas phase (P = 1 atm; T = 373 K) hydrogenation of (tertiary alkynol) 2-methyl-3-butyn-2-ol (MBY) and (secondary) 3-butyn-2-ol (BY) over a series of carbon (C), *non*-reducible (Al_2O_3 and MgO) and reducible (CeO_2 and ZnO) supported mono- (Pd (0.6-1.2% wt.) and Zn (1% wt.)) and bi-metallic Pd-Zn (Pd:Zn mol ratio = 95:5, 70:30 and 30:70) catalysts synthesised by deposition-precipitation and colloidal deposition. The catalysts have been characterised by H_2 chemisorption, hydrogen temperature-programmed desorption (H_2-TPD), specific surface area (SSA), X-ray photoelectron spectroscopy (XPS) and transmission (TEM) and scanning transmission electron microscopy (STEM) analyses. Reaction over these catalysts generated the target alkenol (2-methyl-3-buten-2-ol (MBE) and 3-buten-2-ol (BE)) through partial hydrogenation and alkanol (2-methyl-butan-2-ol (MBA) and 2-butanol (BA))/ketone (2-butanone (BONE)) as a result of full hydrogenation and double bond migration. The catalysts exhibit a similar Pd nanoparticle size (2.7 ± 0.3 nm) but modified electronic character (based on XPS). Hydrogenation activity is linked to surface hydrogen (from H_2 chemisorption and H_2-TPD). An increase in H_2:Alkynol (from 1→10) results in enhanced alkynol consumption with greater rate in the transformation of MBY (*vs.* BY); H_2:Alkynol had negligible effect on product distribution. Reaction selectivity is insensitive to Pd site electron density with a similar response (S_{MBE} = 65 ± 9% and S_{BE} = 70 ± 8%) over $Pd^{\delta-}$ (on Al_2O_3 and MgO) and $Pd^{\delta+}$ (on C and CeO_2).

A Pd/ZnO catalyst delivered enhanced alkenol selectivity (S_{MBE} = 90% and S_{BE} = 96%) attributed to PdZn alloy phase formation (proved by XRD and XPS) but low activity, ascribed to metal encapsulation. A two-fold increase in consumption rate was recorded for Pd-Zn/Al_2O_3 (30:70) *vs.* Pd/ZnO with similar alloy content (32 ± 4% from XPS), ascribed to a contribution due to spillover hydrogen (from H_2-TPD) where high alkenol selectivity was maintained.

INTRODUCTION

The selective catalytic hydrogenation of alkynols is the main synthetic route to alkenols widely employed as reaction intermediates in the manufacture of fine chemicals (*e.g.* vitamins and anticarcinogenic agents).[1] The process is carried out at industrial scale in pressurised (2-5 bar) batch liquid phase reactors over Pd catalysts.[1] A shift from batch to continuous operation reduces the number of processing steps, which improves environmental performance (E-factor reduction from 23 → 3 $kg_{waste\ generated}\ kg_{product}^{-1}$).[2] Alkynols can be classified based on the number of substituents bonded to the hydroxyl C as primary, secondary and tertiary (*i.e.* one carbon, two or three, respectively). The work to date has primarily focused on hydrogenation of tertiary alkynols.[3] The economic benefits of alkenol production are dependent on catalyst performance, where undesired condensation (to dimers), full hydrogenation (to alkanol) and double bond migration (to ketone) are difficult to fully avoid.[4] Hydrogen uptake/release is undoubtely a critical factor that impacts on activity/selectivity response and is linked to metal dispersion and H_2:Alkynol ratio. The formation of small (<4 nm) well-dispersed Pd nanoparticles is essential for significant hydrogen uptake and hydrogenation activity.[5] Control of metal

dispersion is challenging using conventional catalyst preparation techniques (*e.g.* impregnation or deposition-precipitation) but this can be circumvented by the synthesis of metal colloids with controlled size that are loaded onto a support.[6] The undesired formation of dimers and alkanols can be governed by hydrogen coverage on the catalyst surface[7] which, in turn, can be influenced by the H_2:Alkynol ratio, *i.e.* dimer generation and full hydrogenation are promoted at low (≤1.5)[7] and high ratios (≥2.5)[8], respectively. Alkynol hydrogenation reactions have largely been carried out where the H_2:Alkynol (stoichiometric = 1 to alkenol production) was maintained low (typically = 1×10^{-2} - 2×10^{-2}) in both, liquid and gas phase operation.[9,10] It is, nonetheless, worth flagging the study of Prestianni *et al.*,[11] who examined the (gas phase) hydrogenation of (tertiary) 2-methyl-3-butyn-2-ol (MBY) over unsupported Pd nanocubes using an H_2:Alkynol ratio of 3.

The electronic properties of the Pd site is also an essential consideration that impacts directly on the mode/strength of reactant adsorption.[12] Although this can be effectively modified by the Pd crystal size or the support base-acid/redox properties,[13] it is difficult to establish a direct correlation from the existing literature for optimum alkenol

production. Surface defects (*e.g.* kinks, steps and edges) are prevalent on small (<2.5 nm) palladium nanoparticles[14] and promote undesired -C≡C- over-hydrogenation and/or alkenol double bond migration.[15] On the other hand, (111) planes in larger (>6 nm) Pd^0 nanoparticles favour the formation of dimers.[16] A "support effect" has been reported for supports with modified acid-base properties. Zakarina and co-workers[17] and Bönnemann *et al.*[18] working with several oxide (SiO_2, Al_2O_3, MgO, $CaCO_3$, CeO_2) supported palladium catalysts, linked their observed increased in activity and alkenol selectivity in the batch liquid-phase hydrogenation of MBY and 3-hexyn-1-ol to an increased basicity of the support that results in the generation of electron-rich Pd nanoparticles. The opposite effect has also been observed, Berguerand and co-workers[19] recorded a drop in activity in the 2-butyne-1,4-diol hydrogenation linked to the presence of $Pd^{\delta-}$ nanoparticles using a wide range of supports (MgO, ZnO, Ga_2O_3,Al_2O_3, ZrO_2, SnO_2, SiO_2). Alkenol selectivity over supported Pd has also been reported to be sensitive to the introduction of a second metal and ascribed to: (i) blockage of Pd surface sites at corners that promote alkanol formation, (ii) electron transfer from/to Pd sites which impacts on the -C≡C-/-C=C- adsorption strength and/or

(iii) alloy formation that induces geometric and electronic modifications.[12] An alloy lead-poisoned Pd/$CaCO_3$ (Lindlard's) catalyst is typically used at industrial scale[20] but there is a pressing need for an alternative formulation due to the high toxicity of Pb. PdZn alloy has shown promise for alkenol production in pressurised batch liquid systems.[8] We have already shown[21] high selectivity in the continuous gas-phase semi-hydrogenation of MBY over an array of Pd/ZnO catalysts (activated to different temperatures), but control of alloy composition was a decided drawback. We have now extended that work to consider a series of Al_2O_3 supported Pd-Zn colloidal catalysts as a means of controlling alloy composition.

Our intended objective in undertaking this study was to provide a systematic analysis of the critical parameters (H_2:Alkynol, characteristics of the support and Pd-Zn alloy) in the synthesis of tertiary and secondary alkenols through partial hydrogenation of the correspondent alkynol. We have selected 2-methyl-3-buten-2-ol (MBE) and 3-buten-2-ol (BE), with multiple applications in the synthesis of vitamins and tocopherols,[1] as model molecules. We have examined the dependence of alkynol hydrogenation on H_2 partial pressure over Pd/Al_2O_3, as a benchmark. We also address the impact of the

nature of the support for Pd supported on a group of carbon, reducible (CeO_2 and ZnO) and *non*-reducible oxides (Al_2O_3, MgO) with modified acid-base properties as well as the effect of alloy formation for an array of Pd-Zn/Al_2O_3 catalysts prepared by colloidal deposition.

EXPERIMENTAL

Catalysts Preparation

MgO, CeO_2, ZnO, 1.2% wt. Pd/Al_2O_3 (denoted Pd/Al_2O_3-I in this work) and 1.0% wt. Pd/C were purchased from Sigma-Aldrich while the Al_2O_3 support was obtained from Alfa Aesar. Laboratory synthesis of Pd/MgO (0.9% wt.), Pd/CeO_2 (0.8% wt.) and Pd/ZnO (1.1% wt.) by deposition-precipitation (with urea as a base) followed a prior procedure.[22] In addition, a series of Al_2O_3 supported colloidal catalysts (Pd/Al_2O_3-II, Zn/Al_2O_3, Pd-Zn/Al_2O_3 (Pd:Zn molar ratios = 95:5, 70:30 and 30:70)) were prepared by deposition of (*ex-situ*) synthesised monodispersed Pd, Zn and Pd-Zn nanoparticles prepared by a solvent (aka. Polyol) method described in detail elsewhere.[23] Briefly, poly-*n*-vinyl pyrrolidone (0.38 g, monomer:metal = 10:1) was mixed with anhydrous

ethylene glycol (60 cm^3) and $ZnCl_2$ in a two-necked round-bottom flask, stirred for 1 h at 353 K and cooled to 273 K in an ice bath (*solution 1*). In a separate two-necked, round-bottom flask, palladium (II) acetate (0.03-0.07 g) was dissolved in 1,4-dioxane (20 cm^3) under vigorous stirring for 2 h (*solution 2*). Both solutions were mixed (under continuous stirring) to ensure homogenization where the pH was adjusted to pH 9–10 by addition of an aqueous NaOH solution (1-2 cm^3, 1 M). The resulting (bright yellow) solution was capped and heated at 373 K under vigorous stirring for 2 h. A change in colour took place (yellow → dark brown) indicative of colloid formation.[24] The solution was cooled (to room temperature) and the colloids purified (with excess acetone, ~1000 cm^3) and redispersed (in MeOH). The nanoparticles were deposited on the Al_2O_3 support by deposition as described previously.[23] Prior to use, the catalysts were sieved (75 μm) and reduced (60 cm^3 min^{-1}, H_2; BOC, ≥99.99%) at 2 K min^{-1} to 373-573 K in order to ensure formation of Pd^0.[25] *Post*-activation, the systems were cooled (to ambient temperature) and passivated (30 cm^3 min^{-1}, 1% v/v O_2/He, 1 h) for (*ex-situ*) characterisation by TEM/STEM and XPS analyses.

Catalyst Characterisation

The Pd and Zn content was determined by inductively coupled plasma-optical emission spectroscopy (ICP-OES) using the commercial Perkin–Elmer Optima 4300 ICP-OES spectrometer. Prior to analysis, the catalysts were treated in concentrated acid (HNO_3, 343 K, 12 h). Specific surface area (SSA), H_2 titration (at room temperature and/or 373 K) and hydrogen temperature-programmed desorption (H_2-TPD) were performed using the CHEM-BET 3000 (Quantachrome) unit. Total SSA was determined using the standard (single point) method. The samples were outgassed (60 cm^3 min^{-1}, He, 373 K, overnight)[26] and cooled (to room temperature). SSA were recorded with a (30 cm^3 min^{-1}) 50% v/v N_2/He flow with pure N_2 (BOC, 99.9%) as an internal standard. Two cycles of N_2 adsorption–desorption (in the flow mode) were employed to determine total SSA. The samples were reduced (17 cm^3 min^{-1}, 5% v/v H_2/N_2, 2 K min^{-1} to 373-573 K) and kept at the final temperature for 1 h. The reduced sample was swept with a flow of N_2 (60 cm^3 min^{-1}, 1.5 h) in order to remove any physisorbed hydrogen and maintained (at 373 K) or cooled (room temperature) to undergo a pulse (30 µl) H_2 titration procedure; there was no detectable H_2 uptake on the support alone. The samples were thoroughly

flushed in N_2 (60 cm^3 min^{-1}, 30 min) and H_2-TPD (50 K min^{-1} to 973 K) was conducted in the same flow. The reproducibility of SSA and H_2 chemisorption/desorption values was within ±10%; the values quoted in this study are the mean. Transmission (TEM) and scanning transmission electron microscopy (STEM) analysis were conducted using a JEOL JEM 2011 TEM and JEOL 2200FS field emission gun-equipped TEM unit, respectively. The specimens were crushed and deposited (dry) onto a holey carbon film supported on a Ni grid (300 Mesh). The surface area-weighted metal diameter (d) quoted in this paper is based on a measurement of up to 800 individual particles, calculated from:

$$d = \frac{\sum_{i} n_i d_i^3}{\sum_{i} n_i d_i^2} \quad \textbf{(1)}$$

where n_i represents number of particles of diameter d_i. Particle size was also determined by room temperature H_2 chemisorption measurements (d_{H_2}; stoichiometric Pd:H = 1).[27] X-ray photoelectron spectroscopy (XPS) analysis was carried out using a Scienta ESCA 300 spectrometer with monochromatised Al-K_α radiation (1486.6 eV). The analyzer pass energy was 150 eV for survey (0–1100 eV) and high-resolution

spectra (over the Pd $3d_{5/2}$, Pd $3d_{3/2}$ and Pd $3p_{3/2}$ core levels). The C 1*s* peak, centered at 284.5 eV, was employed as reference to compensate for charging effects. Spectra curve fitting/quantification employed the Casa XPS software (version 2.3.17), using Shirley background and Gaussian Lorentzian curves (GL30). The band width (FWHM) spanned the range 1.5-2.5 eV while the Pd $3d_{5/2}$ position (-5.26 eV) and intensity relative to Pd $3d_{3/2}$ peak (+1.5-fold) were fixed.[28] The same fitting procedure was employed in determining the Pd $3p_{3/2}$ position, with deconvolution of the O 1*s* peak as described in detail elsewhere.[29]

Catalytic System

The gas phase (P = 1 atm, T = 373 K) hydrogenation of MBY and BY (Sigma-Aldrich, ≥97%) was carried out (*in situ*) *post* catalyst activation in a (continuous) fixed-bed vertical glass reactor (15 mm internal diameter). The reactor was operated under conditions that guaranteed negligible heat and mass transport constrains. A pre-hetaing zone (*i.e.* layer of (1 mm) borosilicate glass beads) served to ensure the vaporisation of the alkynol reactant and that it reached 373 K before contacting the catalyst bed. The

catalyst bed was thoroughly mixed with ground glass (75 μm diameter) to maintain isothermal conditions (±1 K). Bed temperature was monitored (continuously) using a thermocouple inserted in the catalytic bed. A microprocessor controlled infusion pump (Model 100, kd Scientific) was used to deliver a (1-butanol, Sigma-Aldrich, ≥97%) alkynol solution to the reactor *via* a glass/teflon air-tight syringe (Hamilton) and teflon line at a fixed rate. A *co*-current stream of alkynol and H_2 or H_2/N_2 (P_{H_2} = 4 × 10^{-2} – 3 × 10^{-1} atm) was kept at gas hourly space velocity (*GHSV*) = 1 × 10^4 h^{-1} and monitored using a digital flowmeter (Model 520, Humonics). The molar palladium to inlet molar alkynol feed rate ratio (*n/F*) spanned the range 8 × 10^{-6} – 1 × 10^{-4} h. As blank tests, passage of each (alkynol) reactant in a stream of hydrogen through the empty reactor or over the (oxide/carbonaceous) support alone (*i.e.* without catalyst) did not result in any measurable conversion. The condensable reactor effluent was frozen in an ice-bath trap for off-line (capillary) GC analysis (Perkin-Elmer Auto System XL gas chromatograph, FID, Stabilwax 30 m × 0.32 mm i.d., 0.25 μm column (RESTEK), TotalChrom Workstation) and the reactant and product(s) molar fractions were determined from

calibration plots (not shown). The products, 2-methyl-3-buten-2-ol (98%), 2-methyl-butan-2-ol (99%), 3-buten-2-ol (97%), 2-butanol (99.5%) and 2-butanone (99%) were obtained from Sigma-Aldrich and used as received. Alkynol conversion (X_i) was determined by:

$$X_i\ (\%) = \frac{[\text{Alkynol}]_{in} - [\text{Alkynol}]_{out}}{[\text{Alkynol}]_{in}} \times 100 \quad \textbf{(2)}$$

where selectivity in terms of (for example) alkenol ($S_{Alkenol}$) is given by:

$$S_{Alkenol}\ (\%) = \frac{[\text{Alkenol}]_{out}}{[\text{Alkynol}]_{in} - [\text{Alkynol}]_{out}} \times 100 \quad \textbf{(3)}$$

Catalytic activity is also quantified in terms of steady-state (after *ca.* 3 h) alkynol consumption rate (R, $mol_{Alkynol}\ g_{Pd}^{-1}\ h^{-1}$), obtained from time on-stream conversion data.[30] Repeated (up to three separate) catalytic runs with different systems from the same catalyst batch delivered raw data reproducibility and carbon mass balance that was within ±6%.

RESULTS AND DISCUSSION

The selectivity response is crucial as alkynol hydrogen treatment can result in the formation of several intermediates/by-products as shown in Figure 1, which includes the

reaction networks for the transformation of MBY **(I)** and BY **(II)** based on the paths proposed for liquid phase -C≡C- bond hydrogenation.[31] **Step A** represents the target -C≡C- → -C=C- alkenol semi-hydrogenation. Further hydrogenation results in alkanol formation (**Step B**), which has been ascribed to surface alkenol activation (*via* di-δ) on Pd planes.[32] Alkanol can also be generated directly from the alkynol (**Step C**) through -C≡C- dissociative adsorption on Pd surface defects.[33] The formation of dimers (**Step D**) can result from condensation of two semi-hydrogenated alkene species and has been linked to the formation of vinyl radicals ($^{\bullet}CH=CH_2$) on surface Pd planes at H_2:-C≡C- ≤ 1.5[7] and $P_{\text{-C≡C-}}$ ≥ 0.02 kPa[34]. 2-Butanone formation (BONE) (**Step E**) *via* double bond migration and keto-enol tautomerisation is also favoured on palladium surface defects.[15] The catalysts used in this study promoted only hydrogenation (to MBE, MBA, BE and BA) and double bond migration steps (to BONE) under all reaction conditions, whereas no dimerisation was observed in the transformation of MBY and BY unlike previous work.[10]

Effect of Hydroxyl Group Position and Hydrogen Partial Pressure

We first examined the catalytic response of commercial Pd/Al_2O_3-I (used as a benchmark catalyst) in the (gas phase) hydrogenation of tertiary (MBY) and secondary (BY) alkynols, where the inlet hydrogen has been modified from excess (H_2:Alkynol up to 10) to stoichiometric conditions.

Catalyst Characterisation: Pd/Al_2O_3-I

The STEM analysis *post*-activation revealed a highly dispersed palladium phase (see representative image in **Figure 2(I)**) with a preponderance of nanoparticles in the 1-3 nm size range. The histogram in **Figure 2(II)** shows a narrow metal-size distribution and a small mean diameter (d = 3.0 nm). A palladium particle size of d_{H_2} = 3.6 nm was calculated from H_2 chemisorption (see methodology in Experimental section) that is in good aggrement with the value obtained from STEM measurements. The XPS profile over the Pd 3d binding energy (BE) region is given in **Figure 2(III)**. A two doublet system is in evidence for the reduced sample, spanning the range *ca.* 332-344 eV. The Pd $3d_{5/2}$ BE value for the main (79%; **Table 1**) doublet (334.9 eV) is lower than that characteristic

of palladium bulk metal (335.1 eV),[35] suggesting the existence of electron-rich palladium particles ($Pd^{\delta-}$) linked to electron transfer from the alumina support.[36] The appearance of the two secondary (21%) peaks with BE Pd $3d_{5/2}$ = 336.9 eV and Pd $3d_{3/2}$ = 341.2 eV can be attributed to Pd^{2+},[35] due to formation of surface PdO during the passivation step.[37]

Catalytic Response over Pd/Al_2O_3-I

Catalytic activity (R; $mol_{Alkynol}\ g_{Pd}^{-1}\ h^{-1}$) and selectivity ($S_j$; %) in the hydrogenation of MBY **(I)** and BY **(II)** at the same degree of conversion ($X_{Alkynol}$ ~ 25%) is illustrated as a function of H_2:Alkynol molar ratio in **Figure 3**. The experimentally determined hydrogenation rate of the two alkynols increased linearly with increasing H_2 content in the feed. The noncompetitive nature of reactive alkyne/hydrogen adsorption has been established theoretically for 1-butyne hydrogenation in liquid phase over Pd/Al_2O_3[38] and is consistent with experimental work that has demonstrated a first order dependence in hydrogen coverage for the (gas phase) hydrogenation of acetylene[39] but we present here, for the first time, catalytic data for continuous gas phase operation using

functionalised alkynes (alkynols). The hydrogenation rate of the tertiary alkynol (MBY) was (*ca.* 2-fold) greater than that of the secondary (BY) over the entire H_2:Alkynol interval that was examined. Although we could find no comparable published catalytic study for the gas phase hydrogenation of alkynols, Aramendia *et al.*[40] reported a similar two-fold greater hydrogenation rate in the liquid phase (P = 4 bar, T = 306 K) transformation of MBY (compared to BY) over Pd/Sepiolite. The hydrogenation of alkynes has been suggested to proceed through an electrophilic mechanism[41] where the presence of an additional (electron donor) methyl substituent on the -OH carbon (in MBY *vs.* BY) increases electron density at the -C≡C- bond (positive inductive effect) favouring the hydrogen attack.

We observe the formation of products from partial (MBE and BE) and full hydrogenation (MBA and BA) in the transformation of MBY and BY while 2-butanone (BONE) formation from double bond migration was recorded in the conversion of BY. The hydrogen content in the feed did not influence the selectivity response in the conversion of MBY or BY and a similar product distribution was maintained at each H_2:Alkynol (MBY → S_{MBE} = 62 ± 3%, S_{MBA} = 38 ± 3%; BY → S_{BE} = 69 ± 3%, S_{BA} = 19 ±

3%, S_{BONE} = 12 ± 2%). Our results are in agreement with published work showing a similar selectivity for the gas phase hydrogenation of isoprene over a hydrotalcite supported Cu catalyst under conditions of modified hydrogen content (H_2:Reactant = 1-11) in the feed.[42] We observe a lower selectivity to the desired alkenol in the hydrogenation of tertiary MBY (S_{MBE} ~60%) relative to BY (S_{BE} ~70%). This can be ascribed to differences in the alkynol/alkenol adsortpion strength ($K_{Alkynol/Alkenol}$), *i.e.* a stronger adsorption of the -C≡C- functionality (relative to -C=C-) on the Pd surface for BY compared to MBY ($K_{MBY/MBE}$ = 19 *vs.* $K_{BY/BE}$ = 35)[40] favours the desorption of the alkenol intermediate by displacement. The formation of 2-butanol (S_{BA} = 19 ± 3%) was greater than 2-butanone generation (S_{BONE} = 12 ± 2%), *i.e.* preferential hydrogenation (**Steps B+C** in **Figure 1(II)**) relative to double bond migration (**Step E**), which can be linked to the inhibited formation of the π-allyl intermediate involved in the formation of 2-butanone.[43] The results in this section clearly demonstrate that the hydrogen content in the feed had a minor impact on reaction selectivity in the hydrogenation of tertiary (MBY) and secondary (BY) alkynols. We focus our attention then on the role of the support.

Effect of the Support

The acid-base and/or redox chemistry of the support can induce electron transfer[13] from/to the support to the Pd phase resulting in the formation of negatively (electron-enriched) or positively charged palladium nanoparticles which can impact on reactant adsorption/activation and catalytic performance in hydrogenations.[13] In this section, we evaluate the hydrogenation of MBY and BY over Pd supported on reducible and *non*-reducible supports with modified acidity. We consider a series of catalysts with similar Pd loading (0.8-1.2% wt.; **Table 1**) that facilitates a direct comparison to determine the role of the support.

Catalyst Characterisation: Oxide and Carbon Supported Pd Catalysts

The main physico-chemical properties of the oxide and carbon supported Pd catalysts are presented in **Table 1**. STEM analysis of commercial and laboratory synthesised Pd supported systems demonstrates a similar mean particle size of 2.9 ± 0.1 nm (**Table 1**). Consistent (mean) nanoparticle sizes determined from STEM and H_2 chemisorption were obtained for Pd supported on *non*-reducible oxides and carbon (*i.e.* Pd/Al_2O_3-I (3.3

± 0.3 nm), Pd/C (2.9 ± 0.1 nm) and Pd/MgO (3.5 ± 0.5 nm)). A similar metal dispersion (7-10% error) was reported by Mustard and Bartholomew[44] using microscopy and H_2 chemisorption measurements in the analysis of *non*-reducible (Al_2O_3 and SiO_2) supported Ni catalysts. There are discrepancies in the results generated with both techniques for the remaining two Pd supported on reducible oxide (*i.e.* CeO_2 and ZnO) catalysts, a response that suggests some involvement of the support which influences hydrogen uptake. Metal encapsulation and alloy formation are two possible sources that can inhibit uptake, resulting in an over-estimation of metal particle size.[44] The term "encapsulation" can be defined as a partial/total blockage of the catalytic active (metal) sites by a (thin) layer of reduced oxide support [45] and is a documented feature of Pd supported on ZnO *post*-activation (in H_2) to 423 K.[46] Moreover, the incorporation of a second metal (*e.g.* Cu and Ag)[47] to Pd resulted in a reduction in H_2 uptake attributed to alloy formation. The generation of a supported PdZn alloy phase in Pd/ZnO can occur following partial reduction of the ZnO support by hydrogen generated on Pd^0 during thermal treatment in H_2 to $T \geq 373$ K.[48] The positive deviation on the particle size determination on Pd/ZnO can be tentatively linked to partial encapsulation by the ZnO

support and/or PdZn alloy formation that lowers hydrogen chemisorption capacity. Under-estimation of metal size can be the result of H_2 consumption by the support. Indeed, there is reported evidence that have shown room temperature hydrogen spillover for Pd/CeO_2 that results in "partial" reduction of ceria.[49] The application of electron microscopy for the determination of metal nanoparticle size has certain limitations that can result in innacurate size estimation, *e.g.* poor contrast between the metal nanocrystals and the support that results in an over-estimation of the mean particle size and difficulties in the detection of metal particles with sizes <1 nm.[28] Although both (microscopy and chemisorption) techniques should complement each other, our results suggest that the titration analysis for the reducible oxide supported catalysts does not provide a reliable measure of palladium size, STEM gives the more accurate metal size. Hydrogen chemisorption is, however, a key consideration in hydrogenation processes. Hydrogen uptake under reaction conditions (373 K) was considerably lower than that recorded at ambient temperature for all the catalysts, which can be linked to the exothermic nature of hydrogen chemisorption over Pd metal, making the process less favourable as temperature increases.[50] Hydrogen

chemisorption on Pd/Al_2O_3-I, Pd/C and Pd/MgO (1.4 ± 0.2 mmol g_{Pd}^{-1}) was equivalent and in line with values reported elsewhere (0.7-2.4 mmol g_{Pd}^{-1})[51] for supported Pd catalysts with the same metal content. Pd/CeO_2 and Pd/ZnO exhibit the lowest (0.9 mmol g_{Pd}^{-1}) and highest hydrogen chemisorption values (4.7 mmol g_{Pd}^{-1}), respectively, displaying the same trend as previously obtained at room temperature.

The electronic properties of the palladium phase were analysed by XPS over the Pd 3*d* BE region with peak deconvolution, as presented in **Figure 4** for Pd/ZnO, as representative; the results for the Pd $3d_{5/2}$ peaks are shown in **Table 1**. In this region of the $3d_{5/2}$ signals Pd/C, Pd/CeO_2 and Pd/ZnO exhibit a main (50-90%) component with BE (334.7-335.8 eV) close to Pd^0 (335.1 eV)[35] and a secondary (10-22%) peak (BE = 336.9-337.4 eV) that can be ascribed to Pd^{2+} from passivation.[37] The BE associated with the principal Pd $3d_{5/2}$ signal shows a clear dependence on the support. Previous studies have reported a positive shift to higher (+0.6 eV) binding energies with a decrease in metal particle size (from 8 nm to <1 nm)[52] ascribed to a decrease on the electron density of Pd that affects its *d* band.[53] In this study, all the catalysts exhibit an equivalent particle size which suggests that this effect alone cannot account for the

modification of the main Pd $3d_{5/2}$ peak BE. A shift of BE to lower/higher values can also be the result of interactions with the support. Pd/ZnO exhibits a BE (334.7 eV) that is *ca.* 0.4 eV lower than metallic palladium indicative of electron-rich ($Pd^{\delta-}$) active sites which are ascribed to electron donation from the basic support.[54] The presence of $Pd^{\delta+}$ on C and CeO_2 follows from the recorded (0.3-0.7 eV) higher BE (compared to Pd^0) that can be linked to Pd → support electron transfer.[55] The ocurrence of the MgKL_1L_{23} peak originating from the support lies in the region of the $3d_{5/2}$ signal of Pd^0 (335.1 eV)[35] and Pd^{2+} (336.3 eV).[35] Consequently, the electronic properties of the palladium component in Pd/MgO were examined by analysing the binding energy of Pd $3p_{3/2}$,[29] which offers an alternative to the use of a *non*-monochromatised MgKα (1253.6 eV) radiation.[56] Pd/MgO exhibits a Pd $3p_{3/2}$ BE of 530.5 eV which is lower than that characteristic of Pd^0 (531.4 eV),[57] consistent with the presence of $Pd^{\delta-}$. The Pd/ZnO spectrum (**Figure 4**) presents an additional signal at Pd $3d_{5/2}$ of 335.8 eV (**Table 1**) that can be attributed to the occurrence of a PdZn alloy phase.[46] Tew *et al.*,[58] demonstrated (by XRD and XAS) formation of PdZn alloy (at 373 K) on the Pd surface of Pd/ZnO that progresses into the bulk with increasing the temperature.

The characterisation analyses prove formation of nano-scale Pd particles with similar mean size (2.9 ± 0.1 nm) but different electronic properties and hydrogen uptake capacities.

Catalytic Response over Oxide and Carbon Supported Pd Catalysts

The effect of the support on alkynol hydrogenation rate (*R*) and selectivity response is shown in **Figure 5**. A similar hydrogenation rate was obtained in the hydrogenation of MBY (62 ± 5 $mol_{MBY}\ g_{Pd}^{-1}\ h^{-1}$) and BY (36 ± 6 $mol_{BY}\ g_{Pd}^{-1}\ h^{-1}$) over Pd/Al_2O_3-I, Pd/C and Pd/MgO while Pd/ZnO, with the lowest hydrogen uptake (**Table 1**), delivered the lowest MBY (35 $mol_{MBY}\ g_{Pd}^{-1}\ h^{-1}$) and BY (20 $mol_{BY}\ g_{Pd}^{-1}\ h^{-1}$) transformation rate. This result indicates that the nature of the support does not affect considerably hydrogenation rate, which is governed by the hydrogen uptake. Bragina and co-workers,[59] working with a series of oxide supported Pd catalysts, associated their observed increase in diphenylacetylene hydrogenation to higher hydrogen concentration where the nature of the support did not affect the activity/selectivity response. The opposite effect has also been reported, where a greater activity over $Pd/CaCO_3$ (*vs.* Pd/Al_2O_3, Pd/Charcoal and

Pd/CeO_2) was recorded by Bönnemann and co-workers[18] and attributed to the presence of $Pd^{\delta-}$, that lowers the strength of alkyne interaction with palladium sites.[12] Pd/CeO_2 with greater hydrogen chemisorption (**Table 1**) delivered equivalent activity, which further confirms that the additional chemisorbed hydrogen is consumed by the support and does not contribute to hydrogenation activity under the reaction conditions applied.

With respect to product distribution, Pd/ZnO delivered a significantly greater alkenol selectivity (S_{MBE} = 90%; S_{BE} = 96%) compared with the rest of the systems. This suggests that the electronic modifications on Pd catalyst linked to the the interactions with the support are playing a minor role where the increased olefin selectivity over the Pd/ZnO catalyst can be tentatively attributed to PdZn alloy formation and partial encapsulation that serves to decrease Pd coordination number (*i.e.* smaller ensemble size)[60] and (partially) cover palladium defect sites.[61]

Promoting Effect of Zn in Pd for Pd-Zn Colloids Supported on Al_2O_3

We evaluated in this section the possibility of Zn promotion over Pd by deposition (on Al_2O_3) of a series of bimetallic colloids with varying Pd:Zn molar ratios ((95:5), (70:30)

and (30:70)). We compare the results with those obtained over two monometallic (colloidal) Pd/Al_2O_3-II and Zn/Al_2O_3 and examined the effect of PdZn alloy formation for alkynol hydrogenation (using MBY and BY) in catalytic systems with Pd, Zn and PdZn active sites, evaluating individually the contribution of each of them. The catalytic action of three physical mixtures (Pd/Al_2O_3-II+Zn/Al_2O_3) was also considered for comparison purposes.

Catalyst Characterisation: Colloidal Pd and Pd-Zn Supported on Al_2O_3

Pertinent chemical and physical properties of the colloidal catalysts in this study are given in **Table 2**. Representative medium **(I)** and higher (inset in **(I)**) magnification TEM images of Pd-Zn/Al_2O_3 (95:5 **(A)**, 70:30 **(B)**, 30:70 **(C)**) are presented in **Figure 6** and serve to illustrate the nature of metal particle morphology (size and shape) for the four Pd-containing colloidal systems. The catalysts present *pseudo*-spherical metal particles, a typical shape for PVP stabilised Zn and Pd colloids,[62] with similar size distribution (size range 1–6 nm, **Figure 6(II)**) and mean (2.7 ± 0.2 nm; **Table 2**). XPS analysis was carried out to provide some insight into Pd–Zn surface interactions. The results for

Pd/Al_2O_3-II (profile **(I)**), $Pd\text{-}Zn/Al_2O_3$ (95:5) **(II)**, $Pd\text{-}Zn/Al_2O_3$ (70:30) **(III)** and $Pd\text{-}Zn/Al_2O_3$ (30:70) **(IV)** are presented in **Figure 7**; the Pd $3d_{5/2}$ BE are given in **Table 2**. After deconvolution, the Pd $3d_{5/2}$ spectra for the four Pd-containing systems present two peaks characteristic of $Pd^{\delta-}$ (334.8 ± 0.2 eV) and Pd^{2+} (336.9 ± 0.2 eV), similar to those recorded for Pd/Al_2O_3-I (**Figure 2(III)** and **Table 1**) with equivalent metal dispersion, suggesting similar particle size and metal-support interaction that is independent of the preparation method. $Pd\text{-}Zn/Al_2O_3$ presented and additional peak at higher (335.6 ± 0.2 eV) BE characteristic of PdZn alloy[48] with a concomitant decrease in $Pd^{\delta-}$ and increase in PdZn with enhanced Zn content. Hydrogen pulse titration measurements at reaction temperature demonstrate a significantly lower H_2 chemisorption for Pd/Al_2O_3-II relative to Pd/Al_2O_3-I, which can be linked to an adsorption site coverage by the PVP stabiliser in the colloidal system.[63] We observed an equivalent (0.5 ± 0.1 mmol g_{Pd}^{-1}) H_2 uptake for the monometallic Pd/Al_2O_3-II and bimetallic $Pd\text{-}Zn/Al_2O_3$ catalytic systems, indicative of hydrogen uptake by the PdZn alloy, in agreement with published work.[64]

Catalytic Response over Colloidal Pd and Pd-Zn Supported on Al_2O_3

Monometallic Pd/Al_2O_3-II delivers a similar catalytic response than Pd/Al_2O_3-I and exhibits the lowest alkenol selectivity (S_{MBE} = 64%; S_{BE} = 66%) among all the colloidal catalysts subjected to study. Under the same reaction conditions Zn/Al_2O_3 was inactive, which can be attributed to the incapacitity of zinc for hydrogen adsorption/activation,[65] consistent with the absence of hydrogen uptake at reaction temperature (**Table 2**). The catalytic response for the Pd/Al_2O_3-II+Zn/Al_2O_3 physical mixtures was demonstrated under conditions where the Pd content was kept constant in the catalytic bed and the Pd:Zn mol ratio varied (95:5, 70:30 and 30:70) by adding different quantities of the Zn/Al_2O_3 catalyst. The results shown in **Figure 8** for the hydrogenation of MBY **(I)** and BY **(II)** demonstrate that, for this operational window, the activity over the three Pd/Al_2O_3-II+Zn/Al_2O_3 combinations coincide with that recorded over Pd/Al_2O_3-II (*i.e.* 124 ± 7 $mol_{MBY}\ g_{Pd}^{-1}\ h^{-1}$; 66 ± 4 $mol_{BY}\ g_{Pd}^{-1}\ h^{-1}$). Moreover, product distribution over the three physical mixtures was also similar to that observed for Pd/Al_2O_3-II (*i.e.* S_{MBE} = 63 ± 2%, S_{MBA} = 37 ± 1%; S_{BE} = 68 ± 2%, S_{BA} = 20 ± 1%, S_{BONE} = 13 ± 1%). This suggests that introduction of Zn/Al_2O_3, as a physical mixture with Pd/Al_2O_3-II, does not have an impact

on catalytic performance, which is governed by the Pd component. The three (bimetallic) Pd-Zn/Al_2O_3 catalysts were tested under similar reaction conditions (*i.e.* constant Pd content in the bed). The results in **Figure 8** show a similar alkynol consumption rate for Pd-Zn/Al_2O_3, Pd/Al_2O_3-II+Zn/Al_2O_3 and Pd/Al_2O_3-II, a result that is consistent with the equivalent hydrogen chemisorption under reaction conditions (0.5 ± 0.1 mmol g_{Pd}^{-1}; **Table 2**). In contrast, the selectivity response is remarkable, in that the three Pd-Zn/Al_2O_3 catalysts promoted a greater selectivity (up to S_{MBE} = 86% and S_{BE} = 92%) to the target alkynol whereas Pd/Al_2O_3-II and Pd/Al_2O_3-II+Zn/Al_2O_3 promoted over-hydrogenation (to alkanol; steps **B** and **C** in **Figure 1**) and double bond migration (to butanone; step **E**) to a significantly greater extent (S_{MBE} ≤ 64% and S_{BE} ≤ 69%); full hydrogenation and double bond migration inhibition was observed with increasing Zn content. The switch from over-hydrogenation/double bond migration (Pd/Al_2O_3-II and physical mixtures) to preferential partial hydrogenation (Pd-Zn/Al_2O_3) is indicative of differences in alkynol interation where preferential -C≡C- → -C=C- occurs on the supported bimetallics. The incorporation of a second metal in bimetallic Pd-containing catalysts can result in geometric and/or electronic modifications,[12] which impacts on

catalytic (activity/selectivity) performance. A Ag →Pd electron donation generates palladium nanocrystals with a partial negative charge ($Pd^{\delta-}$), increasing the rate of triple bond hydrogenation while decreasing the rate of double bond hydrogenation.[66] Moreover, incorporation of Cu has been reported to induce geometrical changes on the Pd active sites leading to a partial blockage of low-coordination metal atoms and/or a decrease in the size of surface Pd ensembles, active sites for over-hydrogenation and/or double bond migration.[67] The increase in alkenol production that we observe can be tentatively attributed to a reduction of $Pd^{\delta-}$ surface concentration (from 80% to 37%, **Table 2**) due to PdZn alloy that decreases the number of palladium atoms on surface ensembles responsible for unselective reactions. We cannot discount a partial coverage of (unselective) low-coordinated Pd kinks and corner sites by the Zn component due to its lower surface tension (0.99 J m^{-2}) relative to Pd (2.03 J m^{-2}).[48] Indeed, at 373 K, Zn atoms can diffuse to the surface and interact with Pd to form a thermodynamically stable PdZn alloy (ΔH = -100.4 kJ mol^{-1}) on Pd planes and/or defects sites.[48] Wang *et al.*,[67] investigated the (liquid phase) hydrogenation of phenylacetylene over a series of Al_2O_3 supported Pd-Zn catalysts (Zn:Pd molar ratios 91:9 - 86:14) and reported the

highest yield to the target olefin ($Y_{Ethylbenzene}$ ~ 90%) at full conversion over the bimetallic system with the highest Zn content ascribed to Pd → Zn electron transfer and PdZn alloy formation that blocks unselective active sites. We provide here, for the first time, the results over a highly active and selective Pd-Zn catalyst for continuous production of secondary and tertiary alkenols.

Catalytic properties of PdZn are sensitive to changes on the support. A similar alkenol selectivity (S_{MBE} = 89 ± 3% and S_{BE} = 94 ± 2%) was recorded for Pd/ZnO and Pd-Zn/Al_2O_3 (30:70) with equivalent PdZn alloy content (32 ± 4%). However, a (2-fold) lower hydrogenation rate was obtained over Pd/ZnO compared to the colloidal catalyst. In contrast, Pd/Al_2O_3-II delivered equivalent activity but lower selectivity to the target alkenol than Pd-Zn/Al_2O_3 (30:70) (**Figure 8**). It should, however, be noted a similar hydrogen uptake for the three catalysts (0.7 ± 0.3 mmol g_{Pd}^{-1}; **Tables 1** and **2**). The hydrogenation of -C≡C- bond-containing chemicals can be elevated by contributions due to spillover hydrogen (atomic hydrogen produced through dissociative adsorption of H_2 on supported metal sites that can migrate to the support). H_2-TPD is a practical measurement that can be used to quantify spillover hydrogen; the H_2 TPD profiles for

Pd/ZnO **(I),** Pd-Zn/Al_2O_3 (30:70) **(II)** and Pd/Al_2O_3-II **(III)** are shown in **Figure 9**. The profile obtained for Pd/ZnO was featureless, indicative of hydrogen consumption by the ZnO support during TPR and consistent with the recorded hydrogen chemisorption measurements, *i.e.* atomic hydrogen spills from the Pd sites to the support resulting in "partial" ZnO → ZnO_{1-x} reduction (at the metal-support interface) with generation of a PdZn alloy phase.[68.] In contrast, over the same temperature range, Pd-Zn/Al_2O_3 (30:70) and Pd/Al_2O_3-II exhibited a broad positive signal (H_2 released) at T > 503 K where the total amount desorbed was similar and significantly greater (by a factor of *ca.*12) than taken up in the titration step. This result indicates that the hydrogen released from the Pd-Zn/Al_2O_3 (30:70) and Pd/Al_2O_3-II samples is predominantely spillover hydrogen formed during the activation step by H_2-TPR.[69]

The elevated rate recorded in this work over Pd-Zn/Al_2O_3 (30:70) can be correlated with surface available reactive hydrogen where H_2-TPD is related to alkynol consumption rate. A similar effect has been reported elsewhere[70] in the hydrogenation of acetylene over a series of Pd-Ag/Al_2O_3 catalysts with a different Ag content, where an

increase in the amount of hydrogen desorbed (based on TPD measurements) resulted in greater catalytic activity.

Conclusions

We have demonstrated that the formation of a Pd-Zn alloy phase can influence catalytic response in Pd promoted gas phase hydrogenation of tertiary (2-methyl-3-butyn-2-ol (MBY)) and secondary (3-butyn-2-ol (BY)) alkynols. Catalyst characterisation of Pd nanoparticle size by (room temperature) H_2 chemisorption and TEM/STEM was carried out where the latter is shown to provide the most reliable results. Hydrogen titration leads to erroneous results due to metal encapsulation, alloy formation and/or consumption by the support. Alkynol consumption rate correlates with H_2 chemisorption capacity. An increase in H_2:Alkynol was accompained by enhanced hydrogenation rate in the conversion of MBY and BY, albeit a similar product composition. The nature of the support (carbon, Al_2O_3, MgO, CeO_2) affects the electronic properties of the Pd phase (proved by XPS) but did not influence significantly catalytic activity or selectivity for a series of catalysts with similar metal nanoparticle size (2.9 ± 0.1 nm). In total

contrast, Pd/ZnO delivered a significantly greater selectivity to the target olefin, which is attributed to the generation of a PdZn alloy (based on XPS). The beneficial role of spillover hydrogen has been established where increased surface hydrogen content enhances alkenol production over Pd-Zn/Al_2O_3 (30:70) compared to Pd/ZnO with similar PdZn alloy content.

Acknowledgements

We acknowledge Prof. C. Baddeley, Dr. F. Grillo and Dr. S. Francis for assistance with XPS measurements and are grateful to M. J. Redondo Reina for her contribution to the work. This research was funded by the Engineering and Physical Sciences Research Council (EPRSC; grant number EP/L016419/1; Ph.D. studentship to Alberto González-Fernández, CRITICAT program), the Spanish Ministerio de Ciencia Innovación y Universidades, Generalitat Valenciana and FEDER (RTI2018-095291-B-I00, MAT2017-87579-R MINECO/FEDER and PROMETEO/2018/076).

References

(1) Bonrath, W.; Medlock, J.; Schütz, J.; Wüstenberg, B.; Netscher, T. Hydrogenation in the

Vitamins and Fine Chemicals Industry - An Overview. In *Hydrogenation*; InTech: Rijeka, 2012; pp 69–90.

(2) Sheldon, R. A.; Arends, I.; Hanefeld, U. Green Chemistry and Catalysis. In *Introduction: Green Chemistry and Catalysis*; Wiley: Weinheim, 2007; pp 1–43.

(3) Ibhadon, A.; Kansal, S. The Reduction of Alkynes Over Pd-based Catalyst Materials-A Pathway to Chemical Synthesis. *J. Chem. Eng. Process Technol.* 2018, *9*, 1–15.

(4) Musolino, M.; De Maio, P.; Donato, A.; Pietropaolo, R. Hydrogenation versus Isomerization in α,β-Unsaturated Alcohols Reactions over Pd/TiO_2 Catalysts. *J. Mol. Catal. A*: *Chem.* **2004**, *208*, 219–224.

(5) Drault, F.; Comminges, C.; Can, F.; Pirault-Roy, L.; Epron, F.; Le Valant, A. Palladium, Iridium, and Rhodium Supported Catalysts: Predictive H_2 Chemisorption by Statistical Cuboctahedron Clusters Model. *Materials (Basel)* **2018**, *11*, 819–832.

(6) Yarulin, A.; Yuranov, I.; Cárdenas-Lizana, F.; Abdulkin, P.; Kiwi-Minsker, L. Size-effect of Pd-(Poly(*N*-vinyl-2-pyrrolidone)) Nanocatalysts on Selective Hydrogenation of Alkynols with Different Alkyl Chains. *J. Phys. Chem. C* **2013**, *117*, 13424–13434.

(7) Bos, A. N. R.; Westerterp, K. R. Mechanism and Kinetics of the Selective Hydrogenation of Ethyne and Ethene. *Chem. Eng. Process.* **1993**, *32*, 1–7.

(8) Cherkasov, N.; Bai, Y.; Rebrov, E. Process Intensification of Alkynol Semihydrogenation in a Tube Reactor Coated with a Pd/ZnO Catalyst. *Catalysts* **2017**, *7*, 1–16.

(9) Deng, D.; Yang, Y.; Gong, Y.; Li, Y.; Xu, X.; Wang, Y. Palladium Nanoparticles Supported on Mpg-C_3N_4 as Active Catalyst for Semihydrogenation of Phenylacetylene under Mild Conditions. *Green Chem.* **2013**, *15*, 2525–2531.

(10) Vernuccio, S.; von Rohr, P. R.; Medlock, J. General Kinetic Modeling of the Selective Hydrogenation of 2-Methyl-3-butyn-2-ol over a Commercial Palladium-based Catalyst. *Ind. Eng. Chem. Res.* **2015**, *54*, 11543–11551.

(11) Prestianni, A.; Crespo-Quesada, M.; Cortese, R.; Ferrante, F.; Kiwi-Minsker, L.; Duca, D. Structure Sensitivity of 2-Methyl-3-butyn-2-ol Hydrogenation on Pd: Computational and Experimental Modeling. *J. Phys. Chem. C* **2014**, *118*, 3119–3128.

(12) Coq, B.; Figueras, F. Bimetallic Palladium Catalysts: Influence of the Co-metal on the Catalyst Performance. *J. Mol. Catal. A*: *Chem.* **2001**, *173*, 117–134.

(13) Crespo-Quesada, M.; Cárdenas-Lizana, F.; Dessimoz, A. L.; Kiwi-Minsker, L. Modern Trends in Catalyst and Process Design for Alkyne Hydrogenations. *ACS Catal.* **2012**, *2*, 1773–1786.

(14) Choi, J.; Zhang, S.; Hill, J. M. Reducibility and Toluene Hydrogenation Activity of Nickel Catalysts Supported on γ-Al_2O_3 and κ-Al_2O_3. *Catal. Sci. Technol.* **2012**, *2*, 179–186.

(15) Bennett, J. A.; Attard, G. A.; Deplanche, K.; Casadesus, M.; Huxter, S. E.; Macaskie, L. E.; Wood, J. Improving Selectivity in 2-Butyne-1,4-diol Hydrogenation Using Biogenic Pt Catalysts. *ACS Catal.* **2012**, *2*, 504–511.

(16) Semagina, N.; Renken, A.; Laub, D.; Kiwi-Minsker, L. Synthesis of Monodispersed Palladium Nanoparticles to Study Structure Sensitivity of Solvent-free Selective Hydrogenation of 2-Methyl-3-butyn-2-ol. *J. Catal.* **2007**, *246*, 308–314.

(17) Zakarina, N. A.; Zakumbaeva, G. D.; Toktabaeva, N. F.; Dyusenbina, B. B.; Litvyakova, E. N.; Kuanyshev, A. S. Monodispersed Palladium Catalysts in the Hydrogenation of Dimethylethynylcarbinol. *Kinet. Catal.* **1983**, *24*, 733–737.

(18) Bönnemann, H.; Brijoux, W.; Siepen, K.; Hormes, J.; Franke, R.; Pollmann, J.; Rothe, J. Surfactant Stabilized Palladium Colloids as Precursors for *Cis*-selective Alkyne-hydrogenation Catalysts. *Appl. Organomet. Chem.* **1997**, *11*, 783–796.

(19) Berguerand, C.; Yuranov, I.; Cárdenas-Lizana, F.; Yuranova, T.; Kiwi-Minsker, L. Size-controlled Pd Nanoparticles in 2-Butyne-1,4-diol Hydrogenation: Support Effect and Kinetics Study. *J. Phys. Chem. C* **2014**, *118*, 12250–12259.

(20) García-Mota, M.; Gómez-Díaz, J.; Novell-Leruth, G.; Vargas-Fuentes, C.; Bellarosa, L.;

Bridier, B.; Pérez-Ramírez, J.; López, N. A Density Functional Theory Study of the 'Mythic' Lindlar Hydrogenation Catalyst. *Theor. Chem. Acc.* **2011**, *128*, 663–673.

(21) González-Fernández, A.; Pischetola, C.; Kiwi-Minsker, L.; Cárdenas-Lizana, F. Partial Hydrogenation of 2-Methyl-3-butyn-2-ol over Pd/ZnO: Effect of Reduction Temperature on Alloy Formation and Catalytic Response. *J. Phys. Chem. C* **2020**, *124*, 3681-3691.

(22) Sokolov, S.; Radnik, J.; Schneider, M.; Rodemerck, U. Low-temperature CO_2 Reforming of Methane over Ni Supported on ZnAl Mixed Metal Oxides. *Int. J. Hydrogen Energy* **2017**, *42*, 9831–9839.

(23) Domínguez-Domínguez, S.; Berenguer-Murcia, Á.; Linares-Solano, Á.; Cazorla-Amorós, D. Inorganic Materials as Supports for Palladium Nanoparticles: Application in the Semi-Hydrogenation of Phenylacetylene. *J. Catal.* **2008**, *257*, 87–95.

(24) Wu, T.; Jiang, T.; Hu, B.; Han, B.; He, J.; Zhou, X. Cross-linked Polymer Coated Pd Nanocatalysts on SiO_2 Support: Very Selective and Stable Catalysts for Hydrogenation in Supercritical CO_2. *Green Chem.* **2009**, *11*, 798-803.

(25) Chen, L. F.; Wang, J. A.; Valenzuela, M. A.; Bokhimi, X.; Acosta, D. R.; Novaro, O. Hydrogen Spillover and Structural Defects in a PdO/Zirconia Nanophase Synthesized through a Surfactant-templated Route. *J. Alloys Compd.* **2006**, *417*, 220–223.

(26) Xinghua, Z.; Tiejun, W.; Longlong, M.; Chuangzhi, W. Aqueous-phase Catalytic Process for Production of Pentane from Furfural over Nickel-based Catalysts. *Fuel* **2010**, *89*, 2697–2702.

(27) Carlsson, A. F.; Bäumer, M.; Risse, T.; Freund, H.-J. Surface Structure of Co–Pd Bimetallic Particles Supported on Al_2O_3 Thin Films Studied Using Infrared Reflection Absorption Spectroscopy of CO. *J. Chem. Phys.* **2003**, *119*, 10885–10894.

(28) Nasar, A. Novel Chitosan-based Nanocomposites for Dye Removal Applications. In *Chitosan-Based Adsorbents for Wastewater Treatment*; Materials Research Foundations; Materials Research Forum LLC: Aligargh, 2018; pp 57–81.

(29) Nolte, P.; Stierle, A.; Balmes, O.; Srot, V.; van Aken, P. A.; Jeurgens, L. P. H.; Dosch, H. Carbon Incorporation and Deactivation of MgO(0 0 1) Supported Pd Nanoparticles during CO Oxidation. *Catal. Today* **2009**, *145*, 243–250.

(30) Cárdenas-Lizana, F.; Gómez-Quero, S.; Hugon, A.; Delannoy, L.; Louis, C.; Keane, M. A. Pd-promoted Selective Gas Phase Hydrogenation of *p*-Chloronitrobenzene over Alumina Supported Au. *J. Catal.* **2009**, *262*, 235–243.

(31) Crespo-Quesada, M.; Yarulin, A.; Jin, M.; Xia, Y.; Kiwi-Minsker, L. Structure Sensitivity of Alkynol Hydrogenation on Shape and Size Controlled Palladium Nanocrystals: Which Sites Are Most Active and Selective?. *J. Am. Chem. Soc.* **2011**, *133*, 12787–12794.

(32) López, N.; Vargas-Fuentes, C. Promoters in the Hydrogenation of Alkynes in Mixtures: Insights from Density Functional Theory. *Chem. Commun.* **2012**, *48*, 1379–1391.

(33) Sárkány, A.; Weiss, A. H.; Guczi, L. Structure Sensitivity of Acetylene-ethylene Hydrogenation over Pd Catalysts. *J. Catal.* **1986**, *98*, 550–553.

(34) Borodziński, A.; Cybulski, A. The Kinetic Model of Hydrogenation of Acetylene–ethylene Mixtures over Palladium Surface Covered by Carbonaceous Deposits. *Appl. Catal. A*: *Gen.* **2000**, *198*, 51–66.

(35) Moulder, J. F.; Chastain, J.; King, R. C. Standard XPS Spectra of Elements. In *Handbook of X-ray Photoelectron Spectroscopy*; Chastain, J., Ed.; Perkin-Elmer Corporation: Minnesota, 1992; pp 118–119.

(36) Tsud, N.; Johánek, V.; Stará, I.; Veltruská, K.; Matolín, V. CO Adsorption on Palladium Model Catalysts: XPS Pd–Al_2O_3 Interaction Study. *Surf. Sci.* **2000**, *467*, 169–176.

(37) Wojcieszak, R.; Genet, M. J.; Eloy, P.; Ruiz, P.; Gaigneaux, E. M. Determination of the Size of Supported Pd Nanoparticles by X-Ray Photoelectron Spectroscopy. Comparison with X-Ray Diffraction, Transmission Electron Microscopy, and H_2 Chemisorption Methods. *J. Phys. Chem. C* **2010**, *114*, 16677–16684.

(38) Alves, J. A.; Bressa, S. P.; Martinez, O. M.; Barreto, G. F. Kinetic Study of the Liquid-

phase Hydrogenation of 1-Butyne over a Commercial Palladium/Alumina Catalyst. *Chem. Eng. J.* **2007**, *125*, 131–138.

(39) Molero, H.; Bartlett, B. F.; Tysoe, W. T. The Hydrogenation of Acetylene Catalyzed by Palladium: Hydrogen Pressure Dependence. *J. Catal.* **1999**, *181*, 49–56.

(40) Aramendia, M. A.; Borau, V.; Jimenez, C.; Marinas, J. M.; Sempere, M. E.; Urbano, F. J.; Villar, L. Study of the Selective Semi-hydrogenation of Various Carbon-carbon Triple Bonds Over a Pd/Sepiolite Catalyst. *Stud. Surf. Sci. Catal.* **1993**, *75*, 2435–2438.

(41) Karavanov, A. N.; Gryaznov, V. M. Effect of the Structure of Substituted Propargyl and Allyl Alcohols on the Rate of Their Liquid Phase Hydrogenation on a Pd-Ru Alloy Membrane Catalyst. *Bull. Acad. Sci. USSR, Div. Chem. Sci.* **1989**, *38*, 1593–1596.

(42) Bridier, B.; Karhánek, D.; Pérez-Ramírez, J.; López, N. Molecular Understanding of Enyne Hydrogenation over Palladium and Copper Catalysts. *ChemCatChem* **2012**, *4*, 1420–1427.

(43) Karpiński, Z. Catalysis by Supported, Unsupported, and Electron-deficient Palladium. In *Advances in Catalysis*; Academic Press: Warsaw, 1990; Vol. 37, pp 45–100.

(44) Mustard, D. G.; Bartholomew, C. H. Determination of Metal Crystallite Size and Morphology in Supported Nickel Catalysts. *J. Catal.* **1981**, *67*, 186–206.

(45) Fu, Q.; Wagner, T.; Olliges, S.; Carstanjen, H.-D. Metal-oxide Interfacial Reactions: Encapsulation of Pd on TiO_2 (110). *J. Phys. Chem. B* **2005**, *109*, 944–951.

(46) Sárkány, A.; Zsoldos, Z.; Furlong, B.; Hightower, J. W.; Guczi, L. Hydrogenation of 1-Butene and 1,3-Butadiene Mixtures over Pd/ZnO Catalysts. *J. Catal.* **1993**, *141*, 566–582.

(47) Nieuwenhuys, B. E. Chemistry on Single Crystal Surfaces of Pt and Pd Alloys. *Surf. Rev. Lett.* **1996**, *3*, 1869–1888.

(48) Armbrüster, M.; Behrens, M.; Föttinger, K.; Friedrich, M.; Gaudry, É.; Matam, S. K.; Sharma, H. R. The Intermetallic Compound ZnPd and Its Role in Methanol Steam

Reforming. *Catal. Rev.* **2013**, *55*, 289–367.

(49) Bensalem, A.; Bozon-Verduraz, F. F.; Perrichon, V. Palladium-ceria Catalysts : Reversibility of Hydrogen Chemisorption and Redox Phenomena. *J. Chem. Soc. Faraday Trans.* **1995**, *91*, 2185–2189.

(50) Bond, G. C. *Metal-Catalyzed Reactions of Hydrocarbons*; Springer US: New York, 2006.

(51) Monteiro, R. S.; Dieguez, L. C.; Schmal, M. The Role of Pd Precursors in the Oxidation of Carbon Monoxide over Pd/Al_2O_3 and $Pd/CeO_2/Al_2O_3$ Catalysts. *Catal. Today* **2001**, *65*, 77–89.

(52) Nosova, L. V.; Stenin, M. V.; Nogin, Y. N.; Ryndin, Y. A. EXAFS and XPS Studies of the Influence of Metal Particle Size, Nature of Support and H_2 and CO Adsorption on the Structure and Electronic Properties of Palladium. *Appl. Surf. Sci.* **1992**, *55*, 43–48.

(53) Baetzold, R. C. Molecular Orbital Description of Catalysis by Metal Clusters. *J. Catal.* **1973**, *29*, 129–137.

(54) Peng, S.-Y.; Xu, Z.-N.; Chen, Q.-S.; Wang, Z.-Q.; Lv, D.-M.; Sun, J.; Chen, Y.; Guo, G.-C. Enhanced Stability of Pd/ZnO Catalyst for CO Oxidative Coupling to Dimethyl Oxalate: Effect of Mg^{2+} Doping. *ACS Catal.* **2015**, *5*, 4410–4417.

(55) Che, C.; Wang, B.; Shan, C.; Chen, H.; Liu, W.; Tang, Y. An Effective Strategy to Prepare Pd–Ag/$MgCO_3$@α-Al_2O_3 Catalyst for Selective Hydrogenation of Acetylene. *Catal. Lett.* **2017**, *147*, 483–490.

(56) Claus, P.; Berndt, H.; Mohr, C.; Radnik, J.; Shin, E.-J.; Keane, M. A. Pd/MgO: Catalyst Characterization and Phenol Hydrogenation Activity. *J. Catal.* **2000**, *192*, 88–97.

(57) Militello, M. C.; Simko, S. J. Palladium Oxide (PdO) by XPS. *Surf. Sci. Spectra* **1994**, *3*, 395–401.

(58) Tew, M. W.; Emerich, H.; van Bokhoven, J. A. Formation and Characterization of PdZn Alloy: A Very Selective Catalyst for Alkyne Semihydrogenation. *J. Phys. Chem. C* **2011**,

115, 8457–8465.

(59) Bragina, G. O.; Smirnova, N. S.; Krivoruchenko, D. S.; Markov, P. V.; Baeva, G. N.; Stakheev, A. Y. Influence of the Support on the Catalytic Characteristics of the Deposited Palladium in the Liquid-phase Hydrogenation of Diphenylacetylene. *Kinet. Catal.* **2017**, *58*, 763–770.

(60) Zhou, H.; Yang, X.; Li, L.; Liu, X.; Huang, Y.; Pan, X.; Wang, A.; Li, J.; Zhang, T. PdZn Intermetallic Nanostructure with Pd–Zn–Pd Ensembles for Highly Active and Chemoselective Semi-hydrogenation of Acetylene. *ACS Catal.* **2016**, *6*, 1054–1061.

(61) Castillejos-López, E.; Agostini, G.; Di Michel, M.; Iglesias-Juez, A.; Bachiller-Baeza, B. Synergy of Contact between ZnO Surface Planes and PdZn Nanostructures: Morphology and Chemical Property Effects in the Intermetallic Sites for Selective 1,3-Butadiene Hydrogenation. *ACS Catal.* **2017**, *7*, 796–811.

(62) Okhlopkova, L. B.; Kerzhentsev, M. A.; Tuzikov, F. V; Larichev, Y. V; Prosvirin, I. P.; Ismagilov, Z. R. Palladium–zinc Catalysts on Mesoporous Titania Prepared by Colloid Synthesis. I. Size Control Synthesis of PdZn Nanoclusters by a Polyol Method. *J. Nanoparticle Res.* **2012**, *14*, 1089/1-13.

(63) Koczkur, K. M.; Mourdikoudis, S.; Polavarapu, L.; Skrabalak, S. E. Polyvinylpyrrolidone (PVP) in Nanoparticle Synthesis. *Dalt. Trans.* **2015**, *44*, 17883–17905.

(64) Tamtögl, A.; Kratzer, M.; Killman, J.; Winkler, A. Adsorption/Desorption of and CO on Zn-modified Pd(111). *J. Chem. Phys.* **2008**, *129*, 224706–224714.

(65) Dent, A. L.; Kokes, R. J. Hydrogenation of Ethylene by Zinc Oxide. I. Role of Slow Hydrogen Chemisorption. *J. Phys. Chem.* **1969**, *73*, 3772–3780.

(66) Huang, W.; McCormick, J. R.; Lobo, R. F.; Chen, J. G. Selective Hydrogenation of Acetylene in the Presence of Ethylene on Zeolite-supported Bimetallic Catalysts. *J. Catal.* **2007**, *246*, 40–51.

(67) Wang, Z.; Yang, L.; Zhang, R.; Li, L.; Cheng, Z.; Zhou, Z. Selective Hydrogenation of

Phenylacetylene over Bimetallic Pd–Cu/Al_2O_3 and Pd–Zn/Al_2O_3 Catalysts. *Catal. Today* **2016**, *264*, 37–43.

(68) Nozawa, K.; Endo, N.; Kameoka, S.; Tsai, A. P.; Ishii, Y. Catalytic Properties Dominated by Electronic Structures in PdZn, NiZn, and PtZn Intermetallic Compounds. *J. Phys. Soc. Japan* **2011**, *80*, 064801/1-13.

(69) Amorim, C.; Wang, X.; Keane, M. A. Application of Hydrodechlorination in Environmental Pollution Control: Comparison of the Performance of Supported and Unsupported Pd and Ni Catalysts. *Chinese J. Catal.* **2011**, *32*, 746–755.

(70) Liu, Y.; Zhao, J.; He, Y.; Feng, J.; Wu, T.; Li, D. Highly Efficient PdAg Catalyst Using a Reducible Mg-Ti Mixed Oxide for Selective Hydrogenation of Acetylene: Role of Acidic and Basic Sites. *J. Catal.* **2017**, *348*, 135–145.

Table 1: Physico-chemical characteristics of the oxide and carbon supported Pd catalysts.

		Pd/Al_2O_3-I	**Pd/C**	**Pd/MgO**	**Pd/CeO_2**	**Pd/ZnO**
Pd content (%wt.)		1.2	1.0	0.9	0.8	1.1
SSA ($m^2\ g^{-1}$)		145	870	95	37	8
d^a / $d_{H_2}{}^b$ (nm)		3.0 / 3.6	2.8 / 3.0	3.0 / 3.9	3.0 / 1.0	2.9 / 5.6
H_2 chemisorption (mmol $g_{Pd}{}^{-1}$)[c]		1.4	1.6	1.2	4.7	0.9
XPS Pd $3d_{5/2}$ binding energies (eV)	Pd^0 (%)	334.9 (79)	335.8 (90)	[d]	335.4 (90)	334.7 (50)
	PdZn (%)	-	-	-	-	335.8 (28)
	Pd^{2+} (%)	336.9 (21)	337.4 (10)	[d]	337.2 (10)	336.9 (22)

[a]value obtained from STEM/TEM measurements; [b]value from room temperature H_2 chemisorption analysis; [c]hydrogen uptake at 373 K; [d]signals recorded at 530.5 eV for Pd^0 or MgO.

Table 2: Physico-chemical characteristics of the Al_2O_3 supported colloidal Pd, Zn and Pd-Zn catalysts.

		Pd/Al_2O_3-II	**Zn/Al_2O_3**	**Pd-Zn/Al_2O_3 (95:5)**	**Pd-Zn/Al_2O_3 (70:30)**	**Pd-Zn/Al_2O_3 (30:70)**
Pd content (% wt.)		0.7	-	1.0	0.8	0.6
Pd:Zn molar ratio		-	0	95:5	70:30	30:70
SSA (m^2 g^{-1})		50	41	42	42	42
H_2 chemisorption (mmol g_{Pd}^{-1})[a]		0.4	[b]	0.5	0.6	0.5
Metal size range (nm)[c]		1-5	-	1-5	1-5	1-6
d (nm)[c]		2.5	-	2.5	2.6	2.9
XPS Pd $3d_{5/2}$ binding energy (eV)	Pd^0 (%)	335.0 (80)	-	334.7 (65)	335.0 (39)	334.9 (37)
	PdZn (%)	-	-	335.5 (5)	335.7 (31)	335.8 (36)
	Pd^{2+} (%)	337.1 (20)	-	336.7 (30)	336.8 (30)	336.7 (27)

[a]hydrogen uptake at 373 K; [b]absence of hydrogen uptake; [c]value obtained from STEM/TEM measurements.

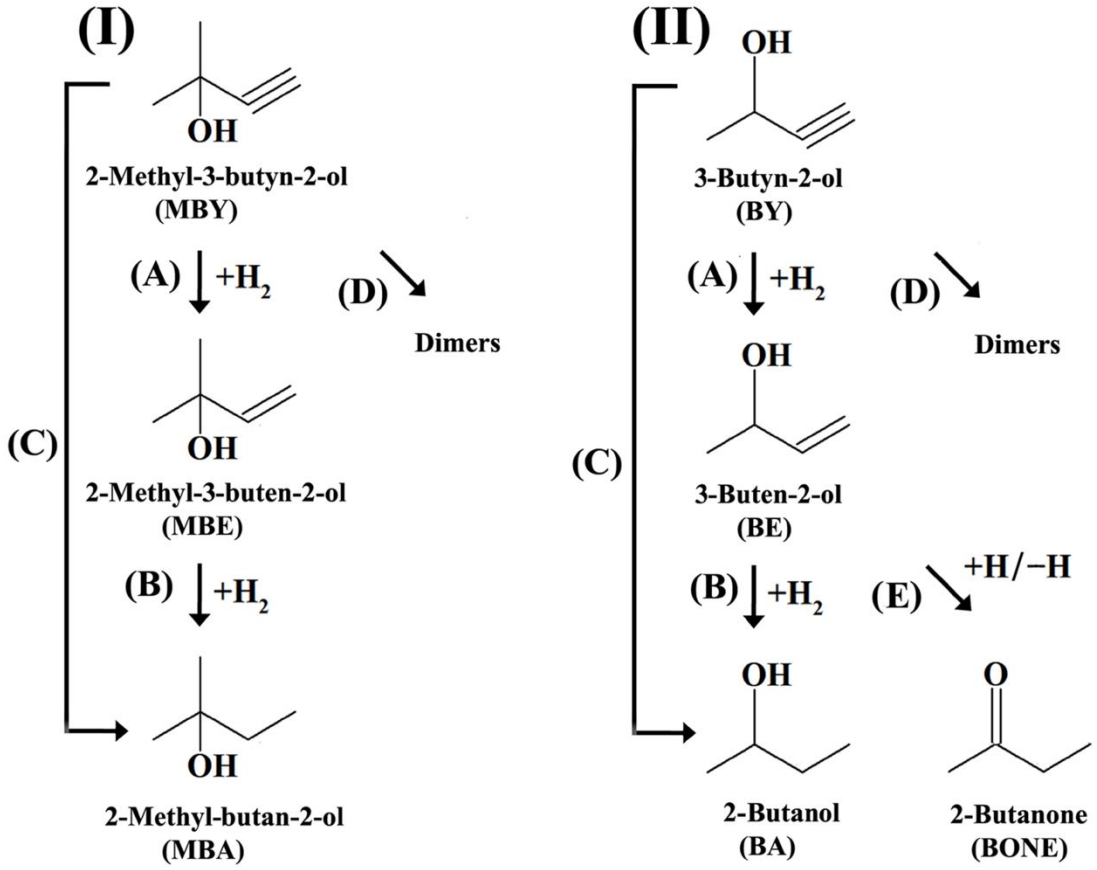

Figure 1: Reaction pathways in the hydrogenation of **(I)** 2-methyl-3-butyn-2-ol (MBY) and **(II)** 3-butyn-2-ol (BY).

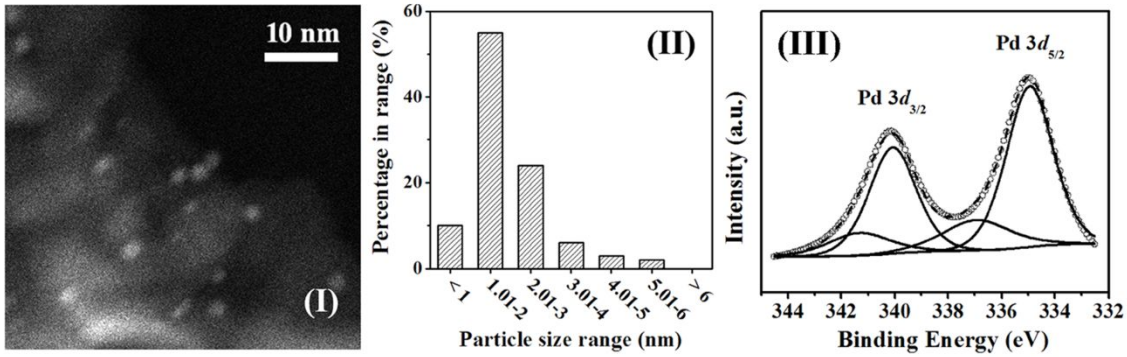

Figure 2: **(I)** Representative high magnitication STEM image with **(II)** associated Pd particle size distribution and **(III)** XPS spectrum over the Pd 3*d* region for Pd/Al_2O_3-I. *Note:* XPS raw data is shown as open simbols (○) while curved fitted and envelope is represented by solid and dashed lines, respectively.

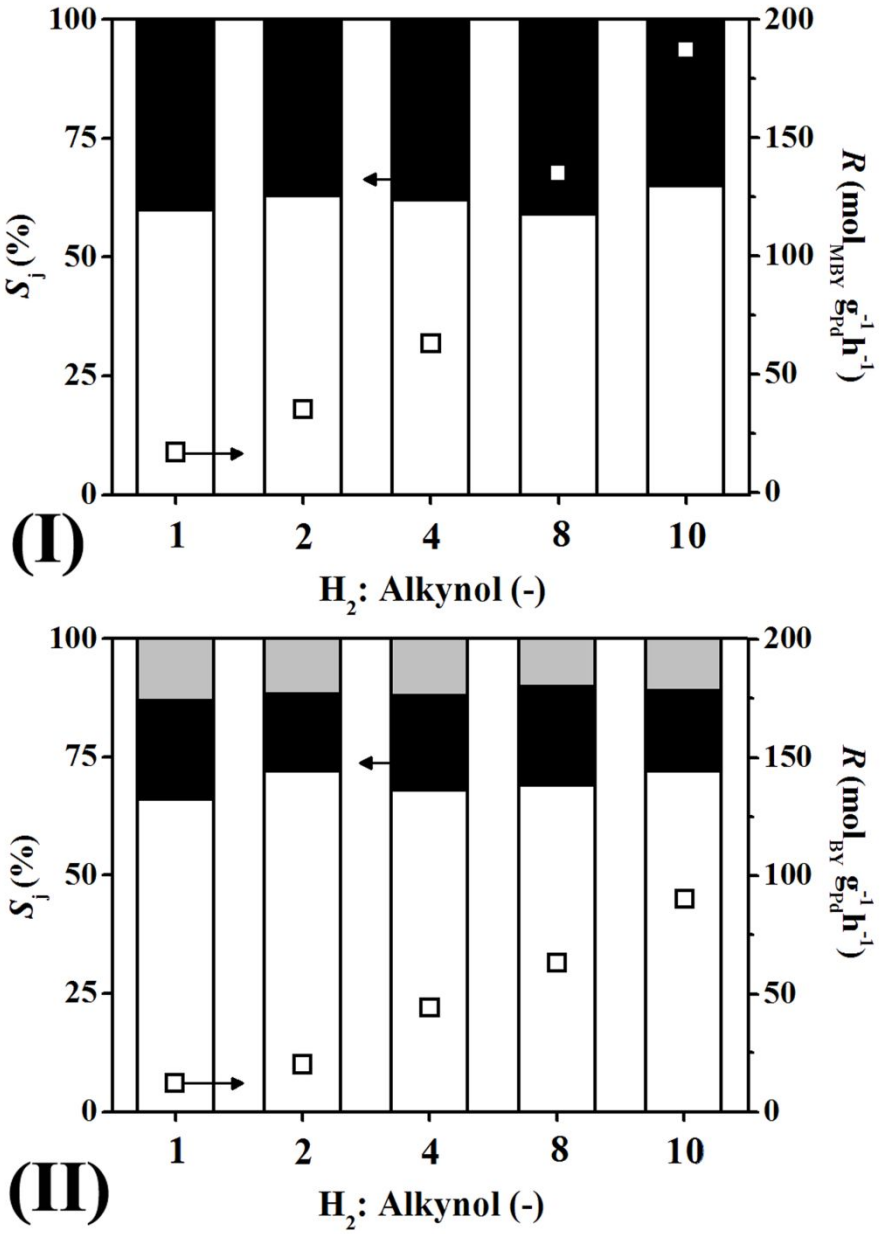

Figure 3: Variation of selectivity (S_j, bars) and alkynol transformation rate (R, □) with H_2:Alkynol molar inlet ratio in the hydrogenation of **(I)** MBY to MBE (open bars) and MBA (solid bars) and **(II)** BY to BE (open bars), BA (solid bars) and BONE (grey bars) over Pd/Al_2O_3-I. *Reaction conditions*: P = 1 atm, T = 373 K, $X_{Alkynol}$ ~ 25%.

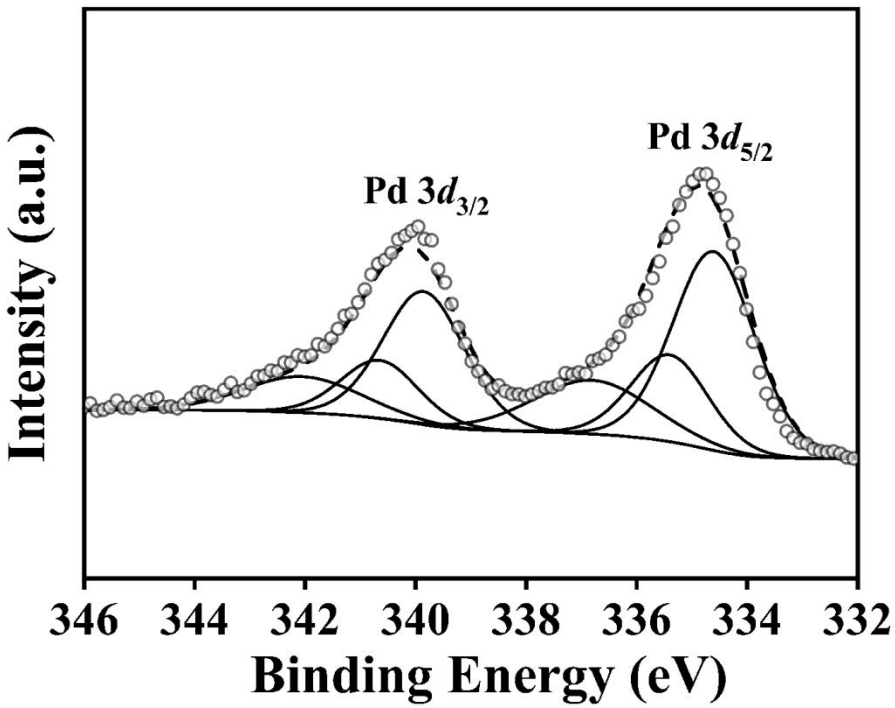

Figure 4: XPS spectrum over the Pd 3*d* region for Pd/ZnO catalyst. *Note:* Raw data is shown as open symbols (○) while curve fitted and envelope is represented by solid and dashed lines, respectively.

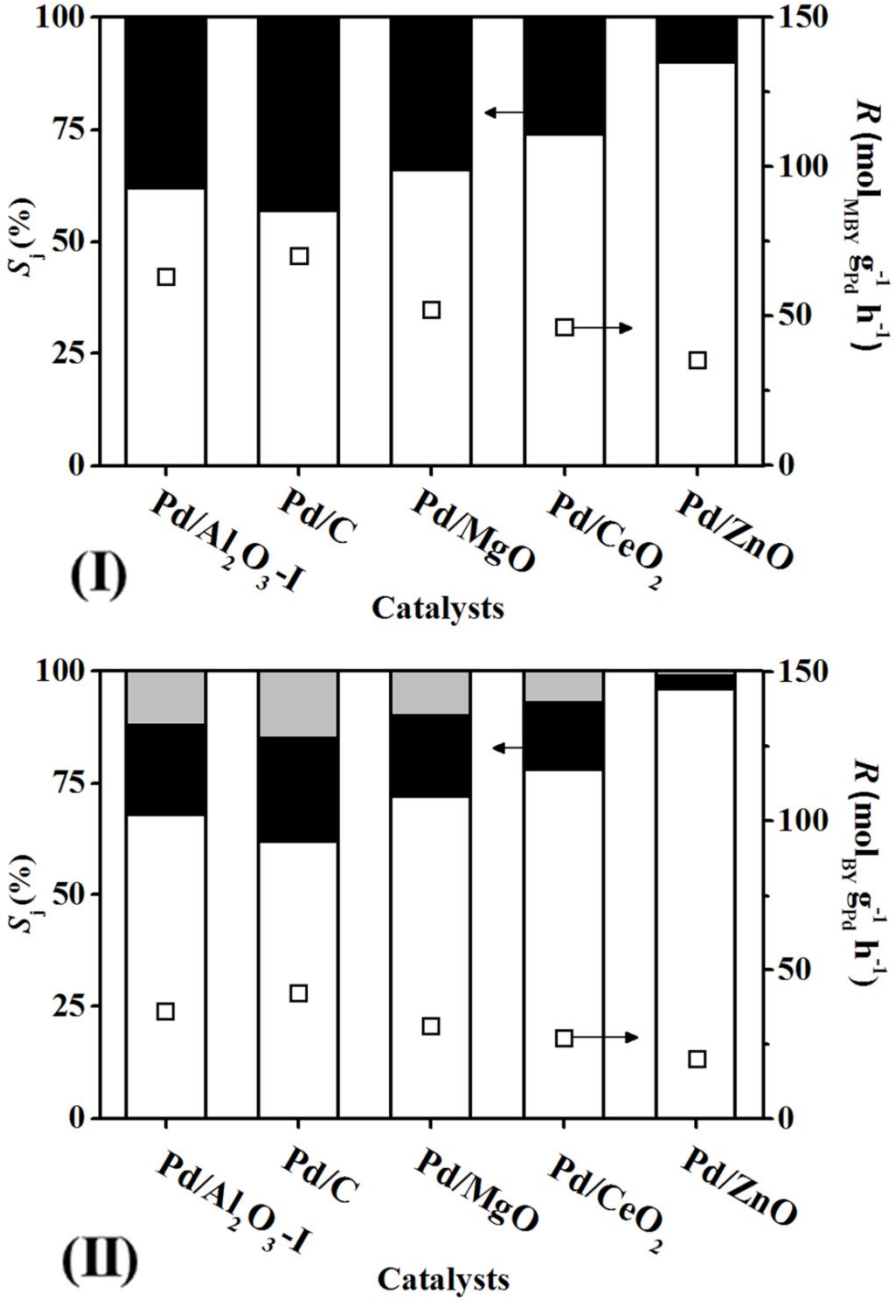

Figure 5: Variation of selectivity (S_j, bars) and transformation rate (R, □) in the hydrogenation of **(I)** MBY to MBE (open bars) and MBA (solid bars) and **(II)** BY to BE (open bars), BA (solid bars) and BONE (grey bars) over a series of oxide and carbon

supported Pd catalysts. *Reaction conditions*: P = 1 atm, T = 373 K, H_2:Alkynol molar inlet ratio = 4, $X_{Alkynol}$ ~ 25%.

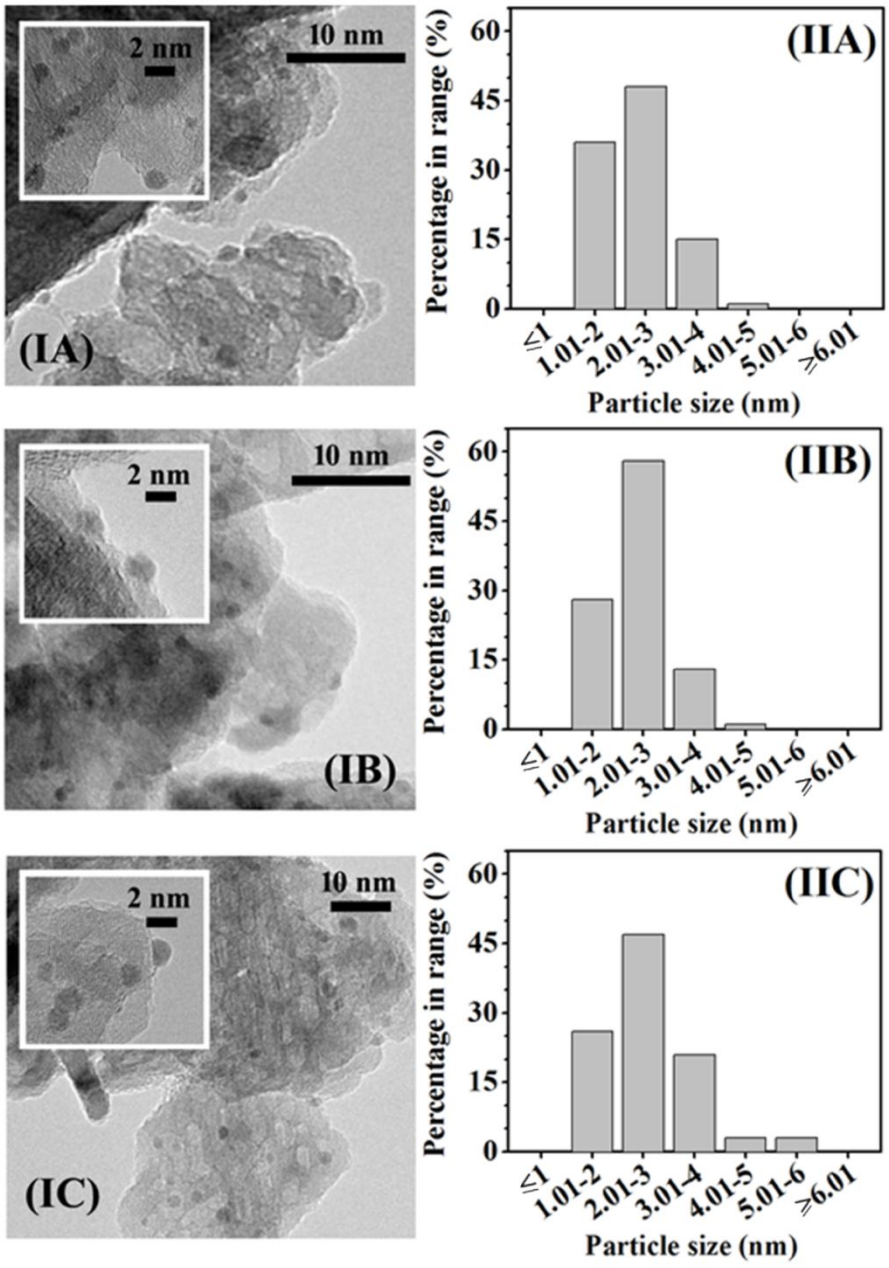

Figure 6: **(I)** Representative medium and high (*inset*) TEM images with **(II)** associated metal particle size distribution for the activated colloidal bimetallic **(A)** Pd-Zn/Al_2O_3 (95:5), **(B)** Pd-Zn/Al_2O_3 (70:30) and **(C)** Pd-Zn/Al_2O_3 (30:70) catalysts.

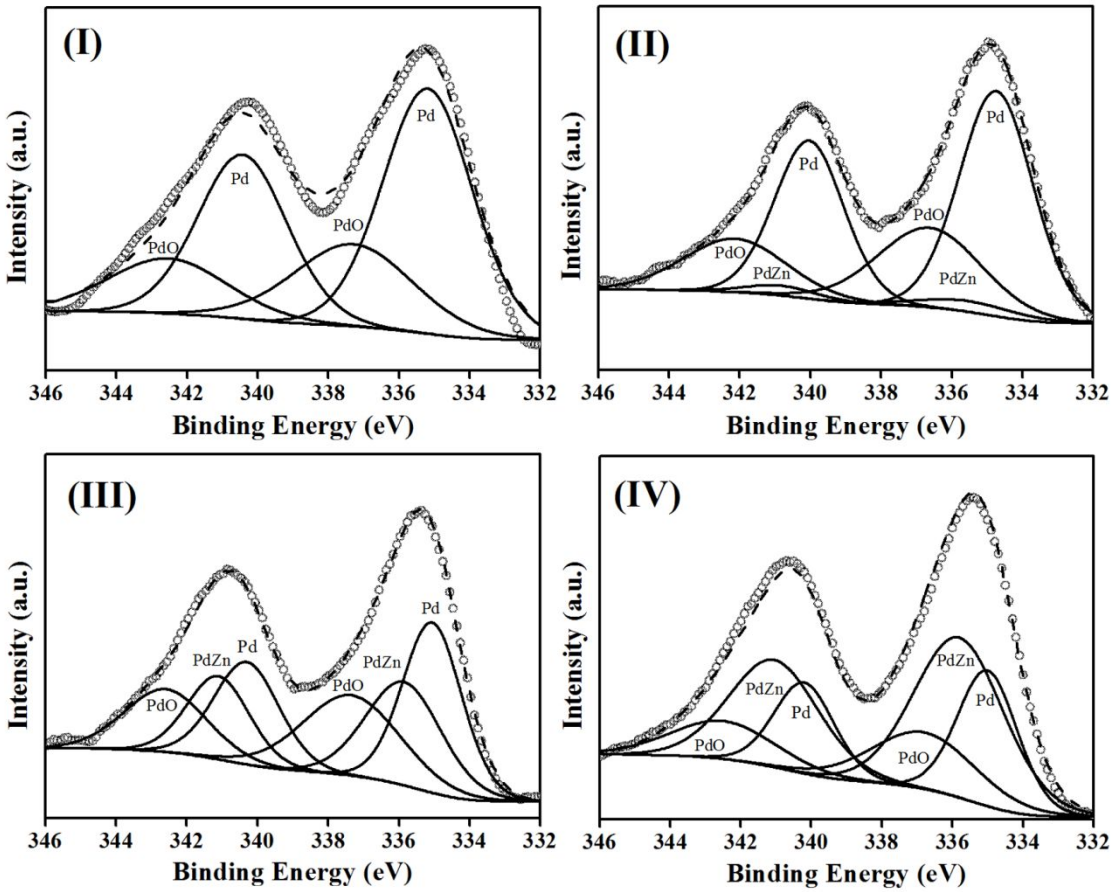

Figure 7: XPS spectra over the Pd 3*d* region for colloidal **(I)** Pd/Al_2O_3-II, **(II)** $Pd\text{-}Zn/Al_2O_3$ (95:5), **(III)** $Pd\text{-}Zn/Al_2O_3$ (70:30) and **(IV)** $Pd\text{-}Zn/Al_2O_3$ (30:70). *Note:* Raw data is shown as open symbols (○) while curve fitted and envelope is represented by solid and dashed lines, respectively.

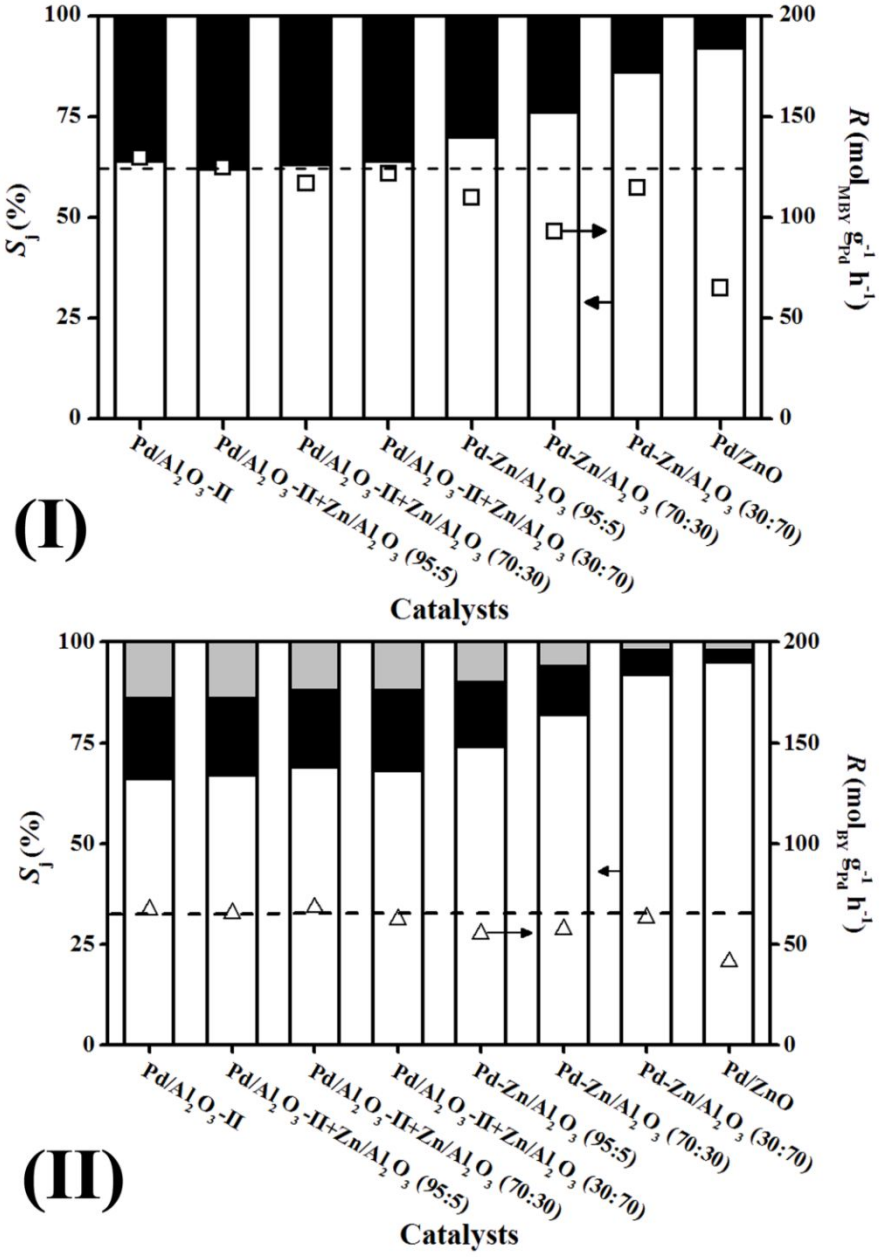

Figure 8: Variation of selectivity (S_j, bars) and transformation rate (R) in the hydrogenation of **(I)** MBY (□) to MBE (open bars) and MBA (solid bars) and **(II)** BY (△) to BE (open bars), BA (solid bars) and BONE (grey bars) over colloidal Pd/Al_2O_3-II and

a series of bimetallic Pd-Zn/Al_2O_3 and (physical mixtures) Pd/Al_2O_3-II+Zn/Al_2O_3 catalysts. *Note:* dashed lines provide a guide to aid visual assessment. *Reaction conditions*: P = 1 atm, T = 373 K, H_2:Alkynol molar inlet ratio = 10, $X_{Alkynol}$ ~ 25%.

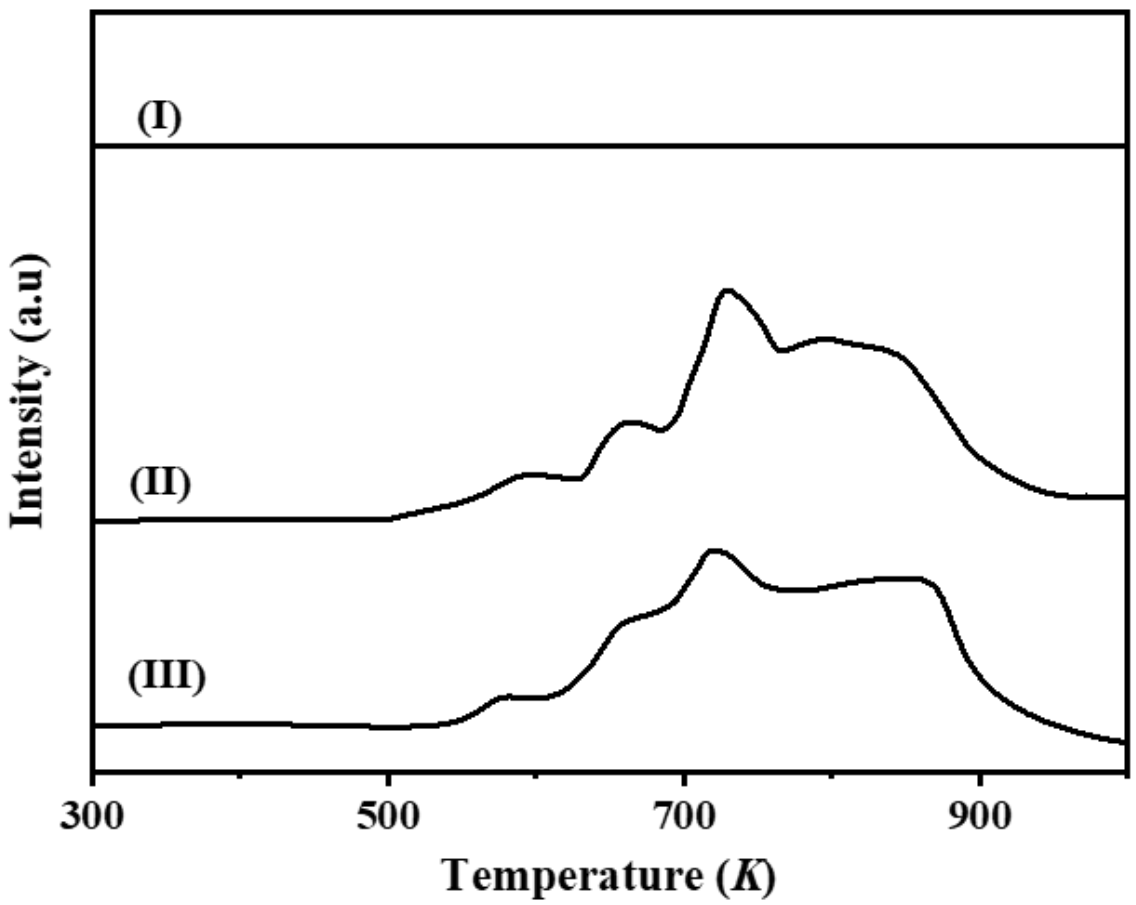

Figure 9: Hydrogen temperature programmed desorption (H_2-TPD) profiles for **(I)** Pd/ZnO and **(II)** Pd-Zn/Al_2O_3 (30:70) and (**III**) Pd/Al_2O_3-II.

Table of Contents

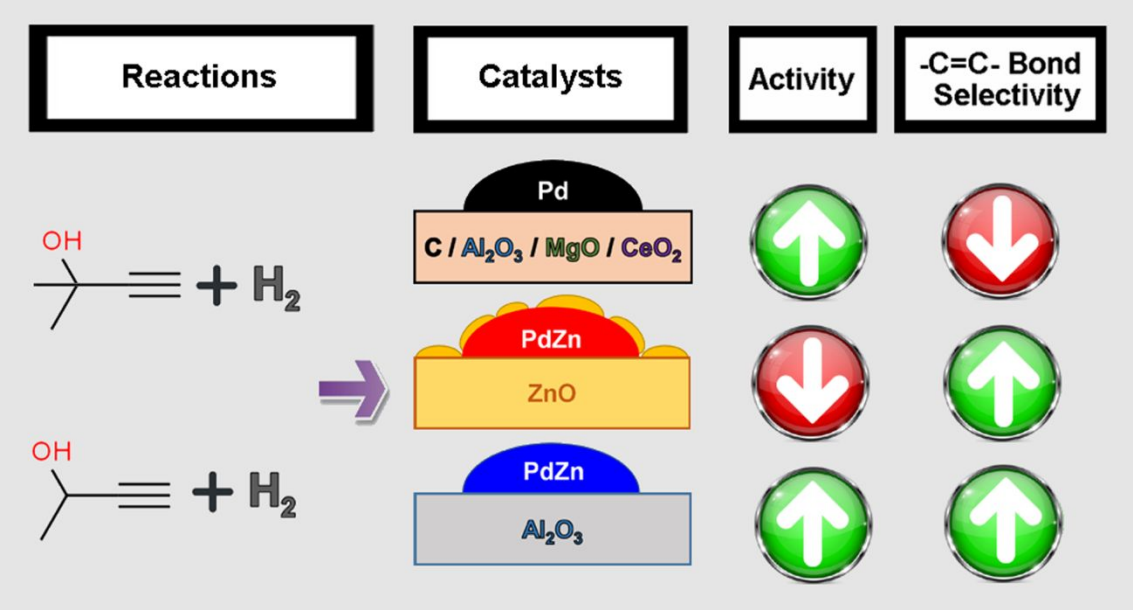

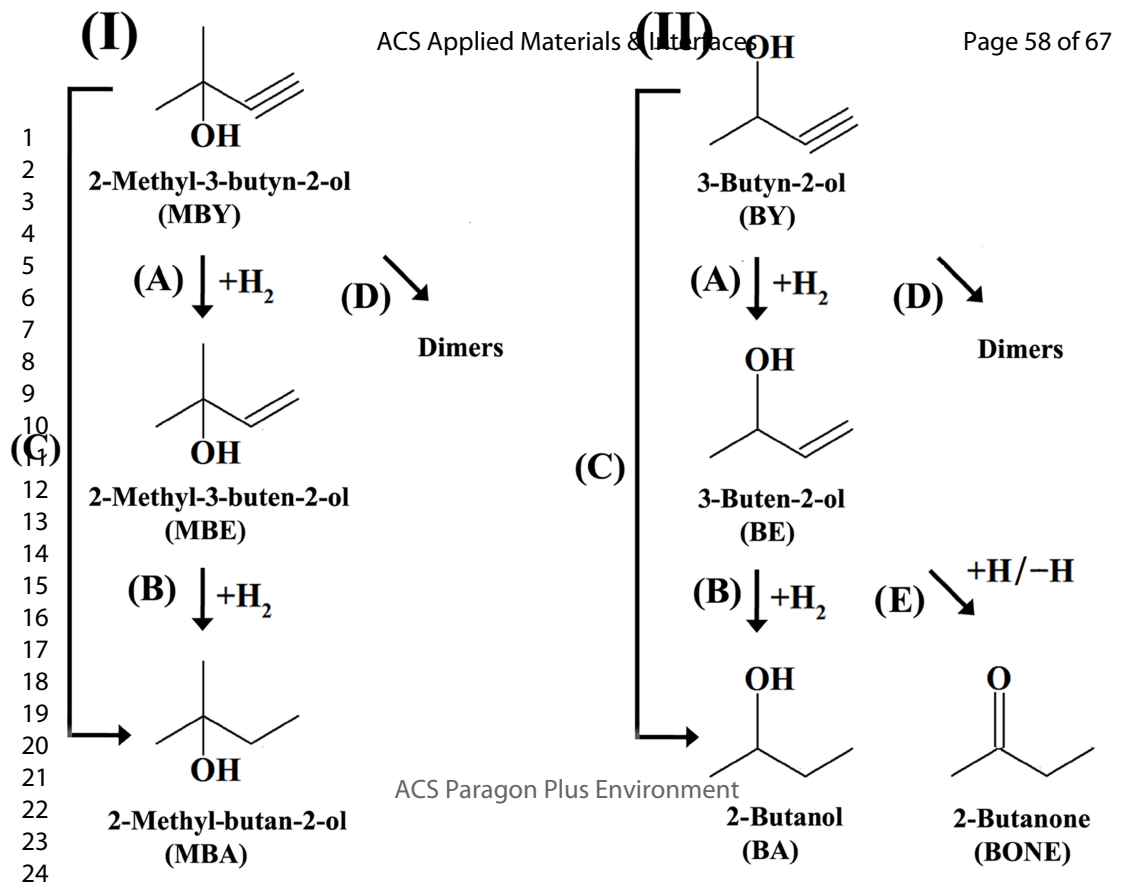

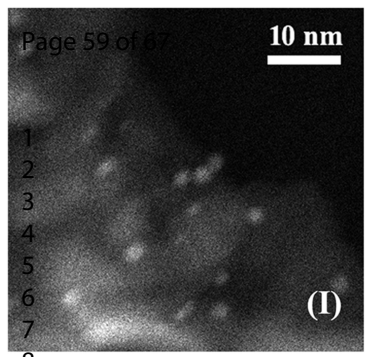

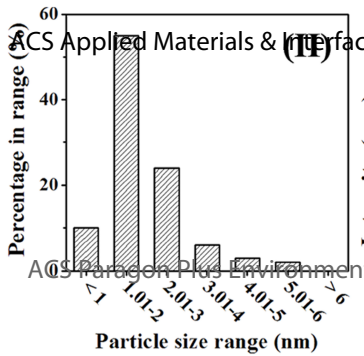

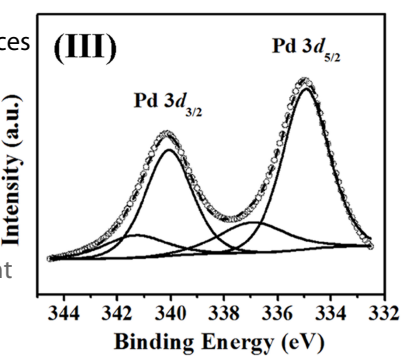

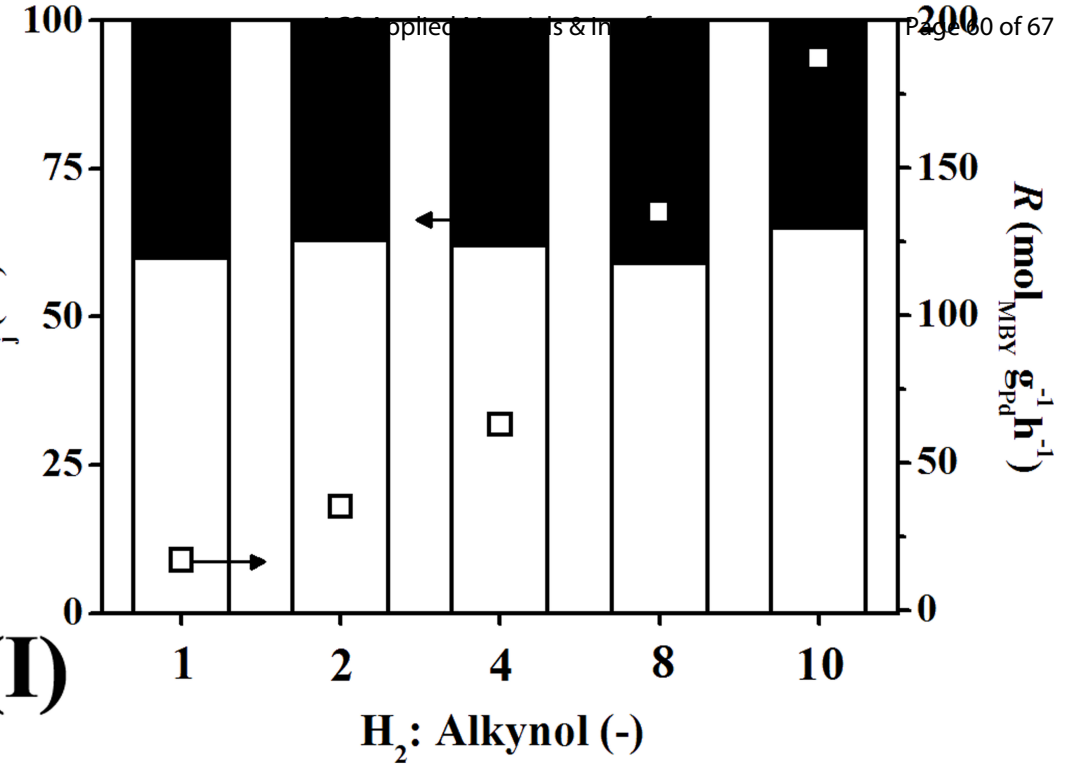
100
75
50
25
0
200
150
100
50
0
S_j (%)
R (mol_{MBY} g_{Pd}^{-1} h^{-1})
1
2
4
8
10
H_2: Alkynol (-)

(I)

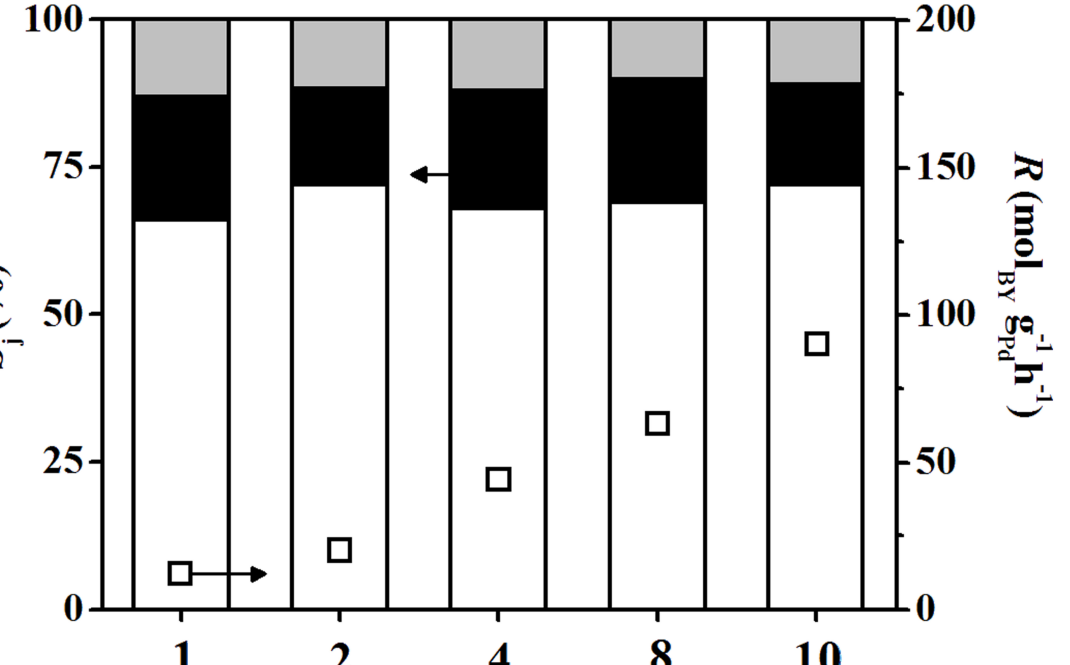
100
75
50
25
0
200
150
100
50
0
S_j (%)
R (mol_{BY} g_{Pd}^{-1} h^{-1})
1
2
4
8
10
H_2: Alkynol (-)

(II)

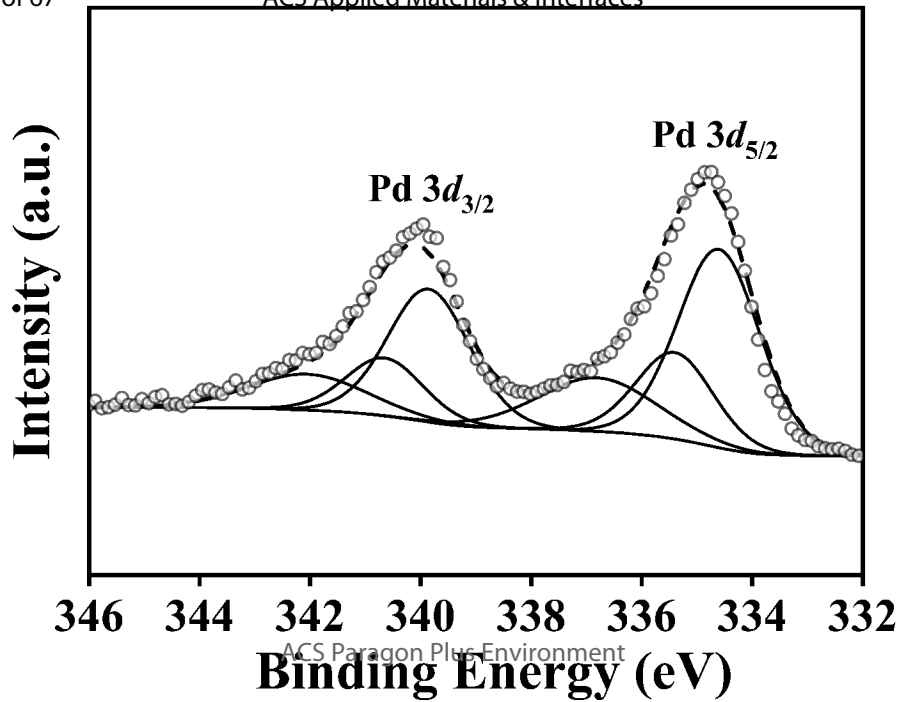

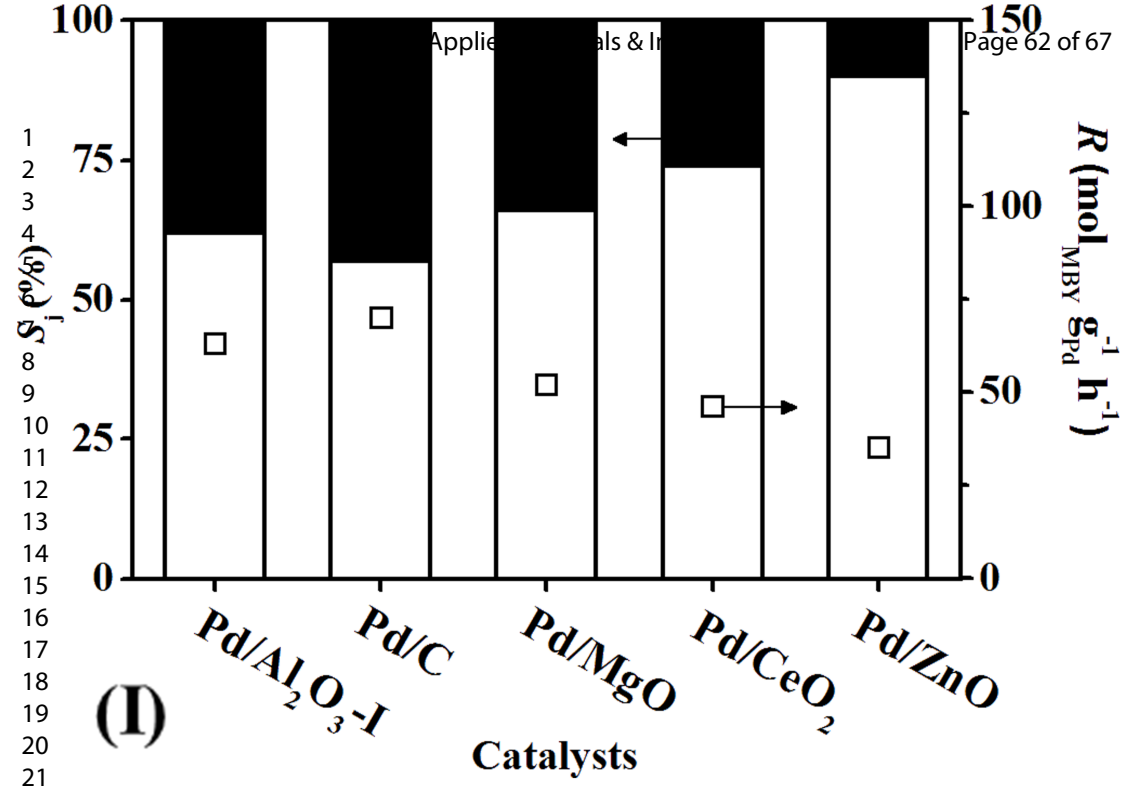
100
75
50
25
0
150
100
50
0
S_j (%)
R (mol_{MBY} g_{Pd}^{-1} h^{-1})
Pd/Al_2O_3-I
Pd/C
Pd/MgO
Pd/CeO_2
Pd/ZnO
(I)
Catalysts

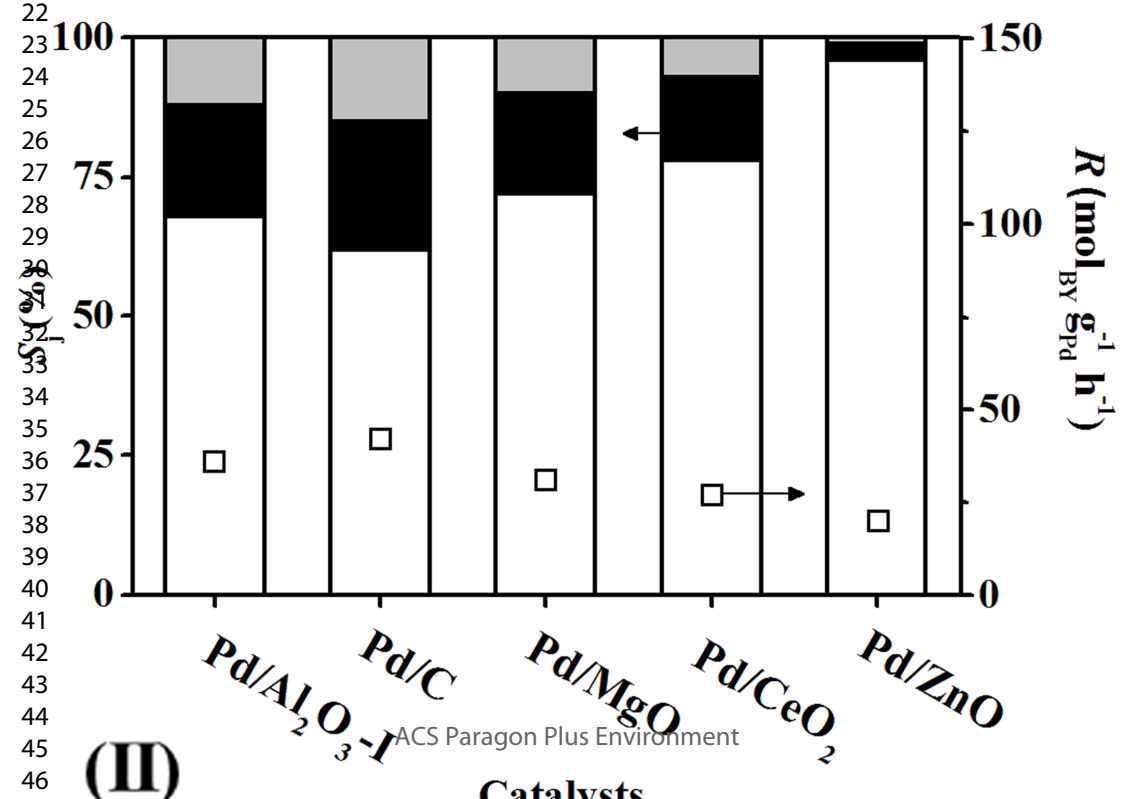
100
75
50
25
0
150
100
50
0
S_j (%)
R (mol_{BY} g_{Pd}^{-1} h^{-1})
Pd/Al_2O_3-I
Pd/C
Pd/MgO
Pd/CeO_2
Pd/ZnO
(II)
Catalysts

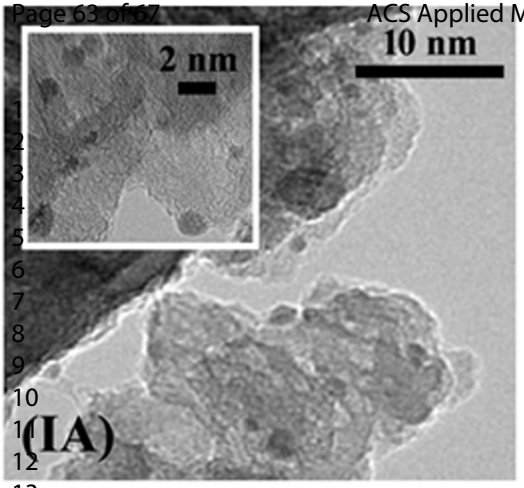
2 nm
10 nm
(IA)

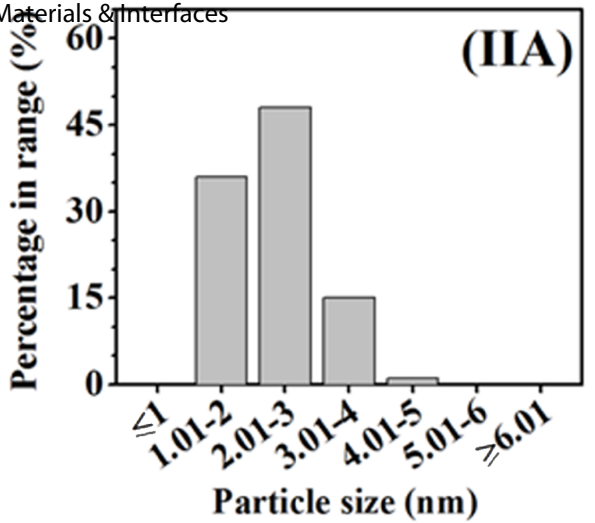
(IIA)
Percentage in range (%)
60
45
30
15
0
≤1
1.01-2
2.01-3
3.01-4
4.01-5
5.01-6
≥6.01
Particle size (nm)

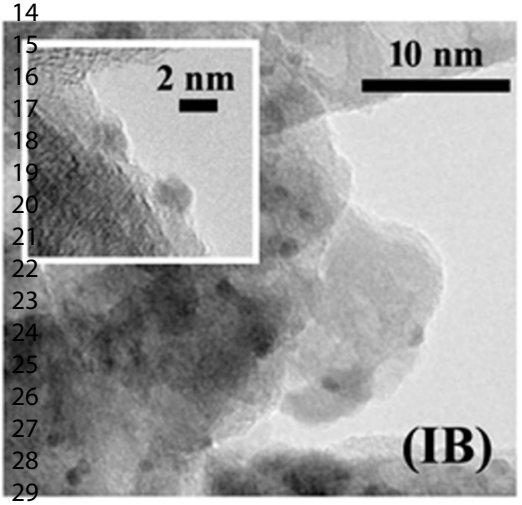
2 nm
10 nm
(IB)

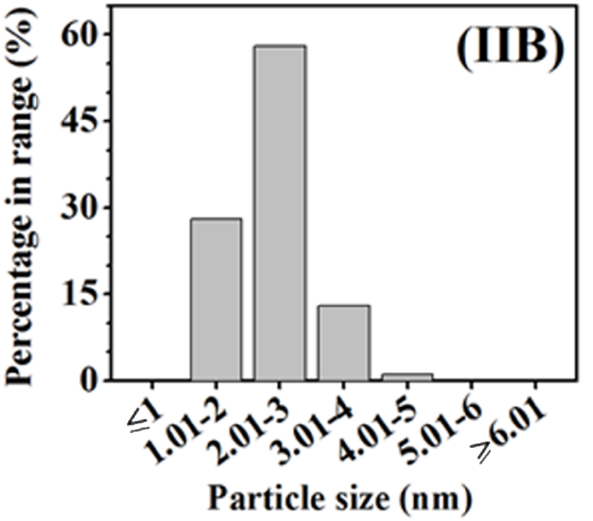
(IIB)
Percentage in range (%)
60
45
30
15
0
≤1
1.01-2
2.01-3
3.01-4
4.01-5
5.01-6
≥6.01
Particle size (nm)

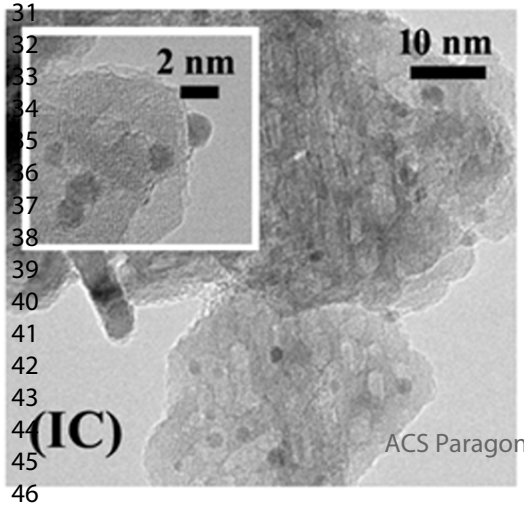
2 nm
10 nm
(IC)

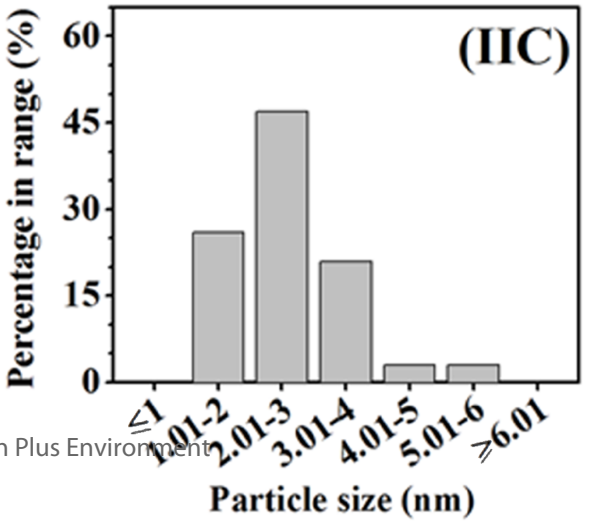
(IIC)
Percentage in range (%)
60
45
30
15
0
≤1
1.01-2
2.01-3
3.01-4
4.01-5
5.01-6
≥6.01
Particle size (nm)

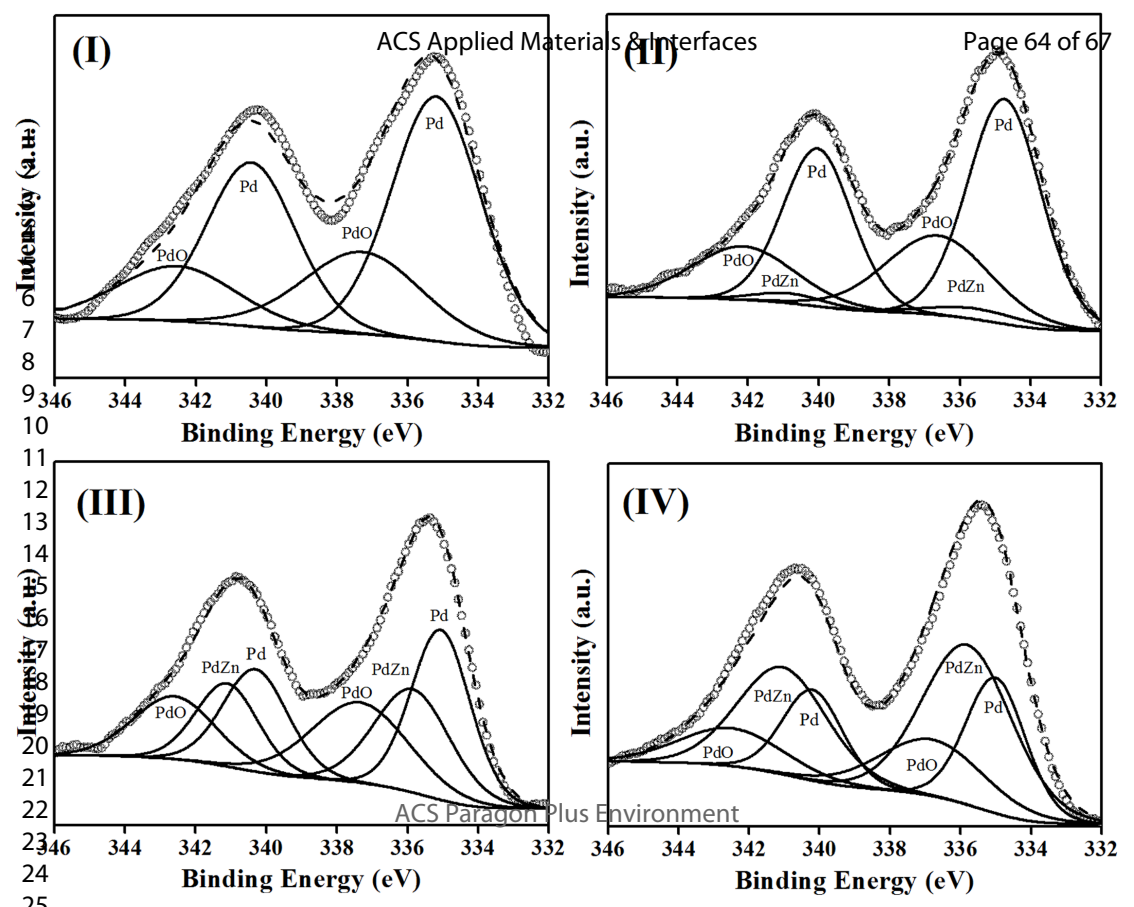

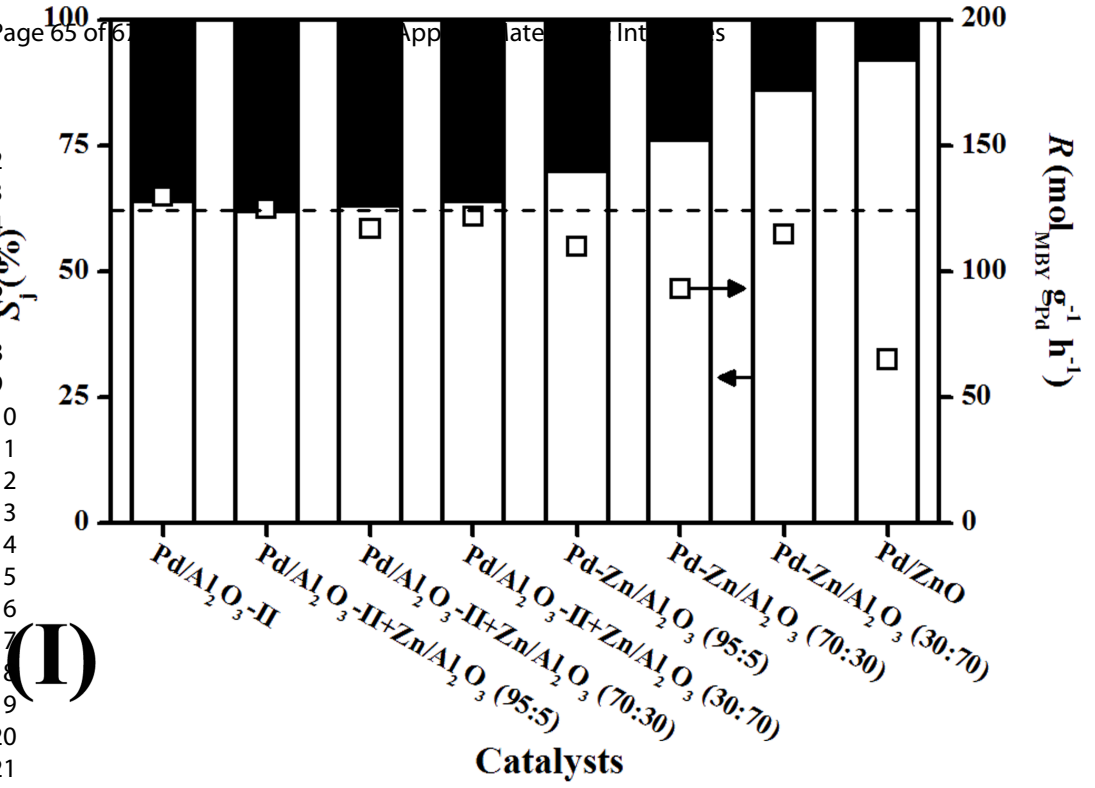

(I)

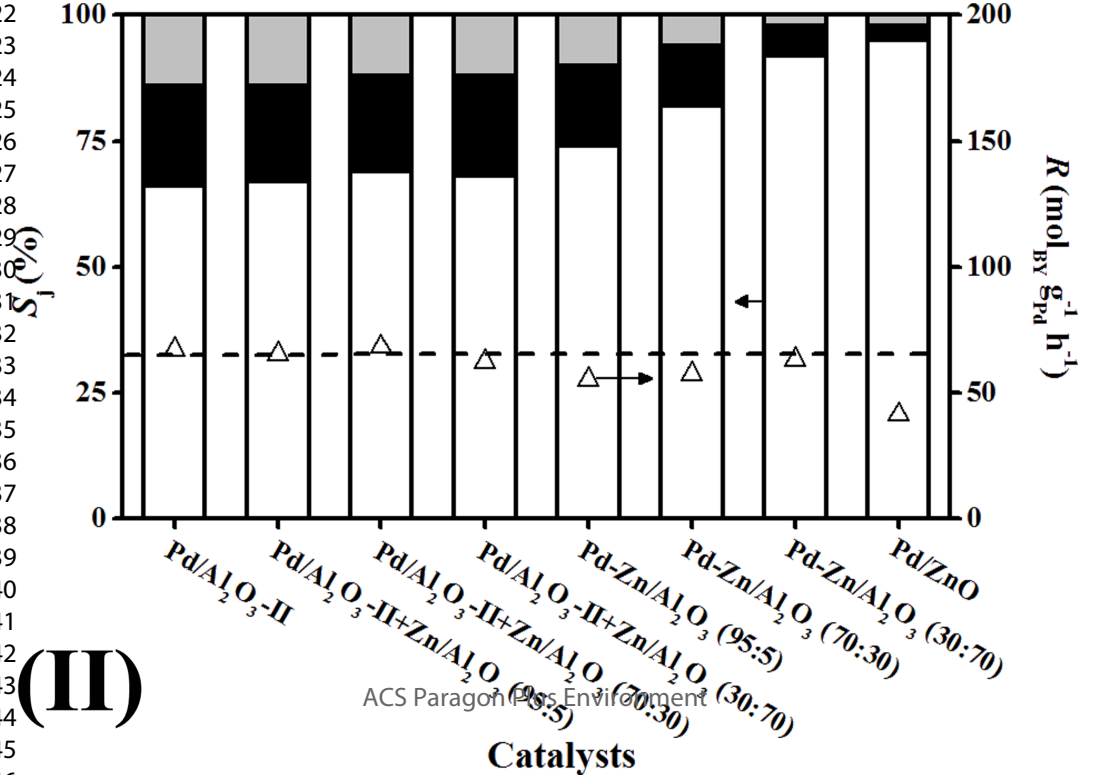

(II)

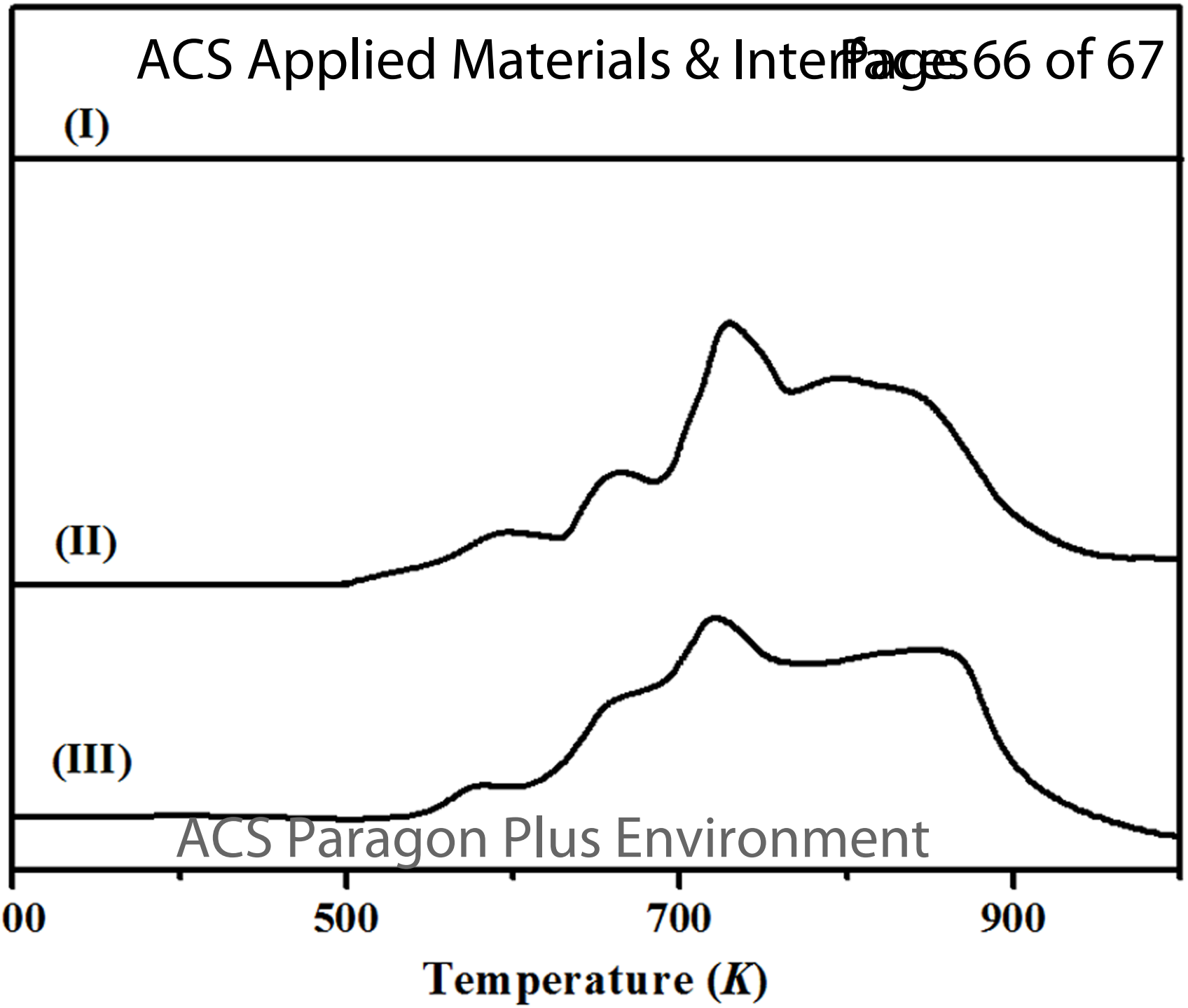

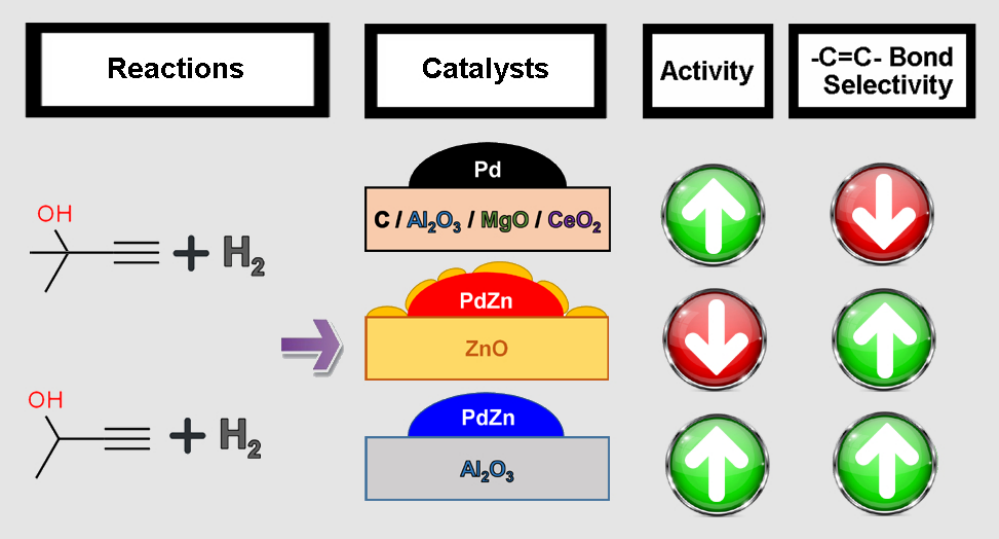

For Table of Contents Only

82x44mm (300 x 300 DPI)